haematologica
Journal of the Ferrata Storti Foundation

Casein kinase II inhibitor CX-4945 synergizes with venetoclax to augment apoptosis by targeting MCL1 in both *in vitro* and *in vivo* models of venetoclax-resistant acute myeloid leukemia

by Muhammad Daniyal, Rajesh Rajaiah, Upendarrao Golla, Marudhu Pandiyan Shanmugam, Morgann Klink, Koby Duke, Katherine Mercer, Preeti Bhadauria, Mohammad Atiqur Rahman, Soumya Iyer, Cesar Aliaga, Hannah Valensi, Jeremy Hengst, Yasin Uzun, Sinisa Dovat, Yi Qiu, Suming Huang and Chandrika Behura

Received: April 16, 2026.
Accepted: November 19, 2026.

Citation: Muhammad Daniyal, Rajesh Rajaiah, Upendarrao Golla, Marudhu Pandiyan Shanmugam, Morgann Klink, Koby Duke, Katherine Mercer, Preeti Bhadauria, Mohammad Atiqur Rahman, Soumya Iyer, Cesar Aliaga, Hannah Valensi, Jeremy Hengst, Yasin Uzun, Sinisa Dovat, Yi Qiu, Suming Huang and Chandrika Behura. Casein kinase II inhibitor CX-4945 synergizes with venetoclax to augment apoptosis by targeting MCL1 in both in vitro and in vivo models of venetoclax-resistant acute myeloid leukemia. Haematologica. 2026 Nov 26. doi: 10.3324/haematol.2026.301063 [Epub ahead of print]

Publisher's Disclaimer.
E-publishing ahead of print is increasingly important for the rapid dissemination of science. Haematologica is, therefore, E-publishing PDF files of an early version of manuscripts that have completed a regular peer review and have been accepted for publication.
E-publishing of this PDF file has been approved by the authors.
After having E-published Ahead of Print, manuscripts will then undergo technical and English editing, typesetting, proof correction and be presented for the authors' final approval, the final version of the manuscript will then appear in a regular issue of the journal.
All legal disclaimers that apply to the journal also pertain to this production process.

Casein kinase II inhibitor CX-4945 synergizes with venetoclax to augment apoptosis by targeting MCL1 in both *in vitro* and *in vivo* models of venetoclax-resistant acute myeloid leukemia

Running title: Novel combination of CK2 inhibitor and venetoclax

Muhammad Daniyal[1#], Rajesh Rajaiah[1,a#], Upendarrao Golla[1], Marudhu Pandiyan Shanmugam[1], Morgann Klink[1,b], Koby Duke[1], Katherine Mercer[1,c], Preeti Bhadauria[1], Mohammad Atiqur Rahman[1,d], Soumya Iyer[1,e], Cesar Aliaga[2], Hannah Valensi[1], Jeremy Hengst[1,2], Yasin Uzun[1,2], Sinisa Dovat[1], Yi Qiu[3], Suming Huang[1], Chandrika G Behura[1*]

[1]Department of Pediatrics, Pennsylvania State University College of Medicine, Hershey, PA, USA

[2]Department of Molecular and Precision Medicine, Pennsylvania State University College of Medicine, Hershey, PA, USA

[3]Department of Cell and Biological Systems, Pennsylvania State University College of Medicine, Hershey, PA, USA

[a]Present address: Center for Drug Evaluation and Research, Food and Drug Administration, Silver Spring, MD 20993, USA.

[b]Present address: AstraZeneca, Gaithersburg, MD 20878, USA.

[c]Present address: Maynard Children's Hospital at ECU Health Medical Center, Greenville, NC 27834, USA.

[d]Present address: Johnson & Johnson Innovative Medicine, Malvern, PA 19355, USA.

[e]Present address: University of Chicago, Chicago, IL 60637, USA.

[#]These authors contributed equally

***Corresponding Author:** Dr. Chandrika Gowda Behura

Email: cxg40@psu.edu; Fax: 717-531-4789

Authors' Contributions: M. Daniyal: Resources, data curation, formal analysis, validation, investigation, visualization, methodology, writing–review and editing. **R. Rajaiah:** Resources, data curation, formal analysis, supervision, validation, investigation, visualization, methodology, writing–original draft, writing–review and editing. **U. Golla:** Data curation, formal analysis, validation, investigation, visualization, methodology, writing–original draft, writing–review and editing. **M. Shanmugam:** Resources, formal analysis, validation, investigation, writing–review and editing. **M. Klink**, **K. Duke**, **K. Mercer, P. Bhadauria, M.A. Rahman, S. Iyer, C. Aliaga:** Resources, investigation, methodology, writing–review and editing. **H. Valensi:** Software, formal analysis, visualization, writing–review and editing. **Y. Uzun:** Data curation, software, formal analysis, visualization, writing–review and editing. **J. Hengst**, **S. Dovat**, **Y. Qiu**, and **S. Huang:** Formal analysis, writing–review and editing. **C.G. Behura:** Conceptualization, resources, data curation, formal analysis, supervision, funding acquisition, writing–original draft, project administration, writing–review and editing.

Funding: This work was supported by grants to CGB from the National Center for Advancing Translational Sciences (KL2 TR002015), Hyundai Hope on Wheels, Four Diamonds Pediatric Cancer Research Fund of the Pennsylvania State University College of Medicine, John Wawrynovic Leukemia Research Scholar Endowment, St. Baldrick's Foundation, the Team Connor, and Rally Foundation.

Acknowledgments: Thanks to Four Diamonds Developmental Therapeutic Preclinical Core and its faculty, Dr. Arati Sharma, and Dr. Diwakar B. Tukaramrao, for providing AML PDX cells. The authors thank the staff of the Institutional Biorepository (RRID:SCR_025728) for sharing de-identified AML patient samples, Department of Comparative Medicine, Flow Cytometry Core (RRID:SCR_021134), and Genome Sciences Core (RRID:SCR_021123) facilities at the Penn State University College of Medicine. The Core services and instruments used in this project were funded, in part, by the Pennsylvania State University College of Medicine via the Office of the Vice Dean of Research and Graduate Students and the Pennsylvania Department of Health using Tobacco Settlement Funds (CURE). The content is solely the responsibility of the authors and does not necessarily represent the official views of the University or College of Medicine. The Pennsylvania Department of Health specifically disclaims responsibility for any analyses, interpretations or conclusions.

Informed Consent Statement: Not applicable.

Data Availability Statement: The RNA-seq data generated in this study have been deposited in the NCBI Gene Expression Omnibus under the accession number GSE342890. The datasets analyzed and novel reagents used during the current study are available from the corresponding author upon request and after a material transfer agreement.

Conflicts of Interest: The authors declare no conflict of interest.

Artificial Intelligence: During the preparation of this manuscript, the authors used Grammarly AI (Grammarly Inc.) to proofread this document for spelling, grammatical errors, and to revise text for improved clarity and readability of specific sections. All AI-assisted text was thoroughly reviewed and edited by the authors, who take full responsibility for the accuracy, integrity, and originality of the final content.

Abstract

Acute myeloid leukemia (AML) remains a therapeutic challenge due to its genetic heterogeneity and the rapid development of resistance to venetoclax (VEN)-based regimens. Resistance is frequently driven by the upregulation of anti-apoptotic proteins such as MCL1 and BCL-XL. Casein kinase II (CK2) is a serine-threonine kinase and a known suppressor of apoptosis in many cancers, including Leukemia. In this study, we identify CK2 as a critical mediator of survival and VEN resistance in AML. Elevated CK2 expression correlates with poor prognosis and high-risk genetic alterations, including TP53 mutation. We demonstrate that the CK2 inhibitor CX-4945 synergizes with VEN across diverse preclinical models, including MLL-rearranged, TP53-mutated, and acquired VEN-resistant (VR) AML. Mechanistically, results are consistent with CK2 inhibition augmenting VEN-mediated apoptosis by decreasing anti-apoptotic MCL1 levels through accelerated proteasomal degradation and increasing mitochondrial "apoptotic priming". *In vivo*, the CX-4945 and VEN combination extended survival in three genetically diverse xenograft models without additional myelotoxicity. CX-4945 also shows synergy with decitabine, 5-Azacytidine, and cytarabine, commonly used agents in VEN-based therapies. CX-4945 has demonstrated a favorable safety profile in early-phase clinical trials across multiple cancer types. These results support clinical testing of CX-4945 in combination with VEN-based therapies for the treatment of high-risk AML.

Keywords: Apoptosis, MCL1, venetoclax resistance, xenograft models

Introduction

Acute myeloid leukemia (AML) is an aggressive hematopoietic malignancy characterized by a dismal prognosis; fewer than 30% of adult patients achieve five-year survival.[1] While cytotoxic chemotherapy and hematopoietic stem cell transplantation (HSCT) remain the foundational treatments, the therapeutic landscape has expanded with the introduction of targeted agents.[2] Venetoclax (ABT-199; VEN), a potent small-molecule BCL-2 antagonist, induces apoptosis by mimicking the BH3 domain of pro-apoptotic proteins, thereby neutralizing the survival mechanisms exploited by AML cells.[3] However, single-agent venetoclax has shown little clinical activity in most AML subtypes. Currently, the FDA has approved VEN in combination with hypomethylating agents (azacytidine or decitabine) or low-dose cytarabine (LDAC) for patients ineligible for intensive induction chemotherapy.[4] However, nearly half of patients receiving these combinations relapse within 18 months.[5] Sustaining durable remission remains a paramount challenge, necessitating novel strategies to stall development of resistance to VEN combination therapy.

Adaptive resistance to VEN-based therapy is multifactorial, of which overexpression of other anti-apoptotic proteins is most common.[6-8] A prominent and actionable mechanism of resistance is the upregulation of MCL1 (Myeloid Cell Leukemia 1), an anti-apoptotic BCL-2 family member.[9] Although MCL1 inhibitors are available, their efficacy is often limited by the concomitant overexpression of BCL-XL and BCL2A1, which provides alternative survival signaling.[10] Furthermore, the clinical utility of selective MCL1 or BCL-XL inhibitors is restricted by dose-limiting toxicities, specifically cardiotoxicity and thrombocytopenia, respectively.[11,12] Additionally, quiescent leukemic stem cells (LSCs) frequently evade conventional therapies, serving as a reservoir for disease relapse.[13] Given the genetic heterogeneity of resistance, there is a critical need for therapeutic targets that remain effective across diverse AML subtypes. It is also important that the additional agent does not have overlapping toxicity, such as myelosuppression. While many studies focus on overcoming resistance to venetoclax in isolation, relapsed AML often exhibits a multidrug-resistant phenotype. Consequently, targeting these diverse resistance mechanisms simultaneously with a single-agent therapy remains a significant clinical challenge and is almost impossible. Additionally, heterogeneity in response testing across genetic subtypes, underscoring the need to test novel agents across multiple AML subtypes and patient-derived models. Casein kinase II (CK2) is a ubiquitously expressed, constitutively active serine-threonine kinase essential for cell survival and

development.[14] The active CK2 holoenzyme is a tetrameric complex consisting of two catalytic subunits (α or α').[15] While the encoding genes (*CSNK2A1*, *CSNK2A2*, and *CSNK2B*) rarely undergo genetic alterations, the enzyme's essential nature is evidenced by the embryonic lethality of *CSNK2A1* deletion in mice.[15,16] However, *CSNK2A1* deletion in the hematopoietic compartment of adult mice does not significantly impair normal hematopoiesis, suggesting a favorable therapeutic window.[17] CK2 phosphorylates over 300 substrates, regulating critical pathways including AKT, Wnt/β-catenin, PTEN, NF-κB, STAT3, p53, and IKAROS.[18-21] Elevated CK2 activity is implicated in the pathogenesis of various hematological malignancies.[22] In AML, CK2 promotes LSC survival by activating survival signaling (AKT, NF-κB, STAT).[23,24] Furthermore, CK2 influences p53 (both wild-type and mutant) through several indirect pathways, suggesting that CK2 inhibition may be effective in p53 mutant AML.[25-27]

Pharmacological inhibition of CK2 with CX-4945 (silmitasertib) has demonstrated *anti-leukemia* activity in AML models without significant myelosuppression.[24] CX-4945 is an orally bioavailable, ATP-competitive inhibitor with a documented safety profile in adult oncology patients.[28] Among available CK2 inhibitors, CX-4945 was the first to enter clinical trials for solid and hematological malignancies due to its high selectivity and potent activity across diverse cancer types.[29] The current clinical trial is evaluating silmitasertib in combination with chemotherapy for pediatric and young adult patients with relapsed/refractory solid tumors (clinicaltrial.gov; NCT03904862). Since CK2 regulates pathways central to AML progression and drug resistance, we hypothesized that CK2 inhibition would augment apoptosis when used in combination with VEN. Given the known inhibitory effect of CK2 on anti-apoptotic drivers of venetoclax resistance such as MCL1 and BCL-XL, we hypothesized that the addition of a CK2 inhibitor will not only augment apoptosis in a VEN-sensitive setting but also partially reverse the VEN-resistant phenotype. In this study, we report the anti-leukemia effect of the CX-4945 and VEN combination using preclinical models representing various AML genetic subtypes, VEN sensitivity profile and elucidate its underlying molecular mechanism.

Methods

The online *Supplementary Appendix* contains detailed experimental methods and materials.

Cell culture

AML cell lines, primary AML patient cells, and patient-derived xenograft (PDX) AML cells were cultured as previously described.[24] Cell lines were routinely confirmed to be negative for mycoplasma contamination and authenticated by short tandem repeat (STR) profiling (Promega, Wisconsin). The clinical characteristics of the AML cells are summarized in **Tables S1-S3**. See *Supplementary Appendix* for reagent details.

Clinical samples

Bone marrow aspirates or peripheral blood samples were obtained from AML patients after informed consent using protocols approved by the Institutional Review Board (IRB #40532) of Penn State College of Medicine. See *Supplementary Appendix* for more details.

Cell viability assays and synergy analysis

The cell viability of AML cells after combinatorial treatment was assessed by Cell Proliferation Reagent WST-1 solution (Sigma-Aldrich, St. Louis). The data was presented as % viability relative to vehicle control. The synergy between two drugs was analyzed using the CompuSyn software and calculated the combination index (CI) to quantitatively determine the effect of drug interactions.[30] See *Supplementary Appendix* for more details.

Transcriptome analysis by RNA-sequencing

The reads were processed, aligned to the human reference genome (hg38), and visualized as previously described.[17] Tools used for functional enrichment analysis were listed in the *Supplementary Appendix*.

BH3 profiling and flow cytometry

Intracellular BH3 profiling was performed as described earlier.[31] The BH3 profiling and flow cytometry were detailed in the *Supplementary Appendix*.

Immunoblotting analysis

The AML cell lines were left untreated or treated with DMSO (vehicle), CX, VEN, and CX+VEN combination at the indicated doses for 2 – 24 h. Whole cell lysates were subjected to immunoblotting analysis with respective primary antibodies as described in the *Supplementary Appendix*.

***In vivo* mice efficacy and safety studies**

All animal experimental protocols were approved by the Institutional Animal Care and Use Committee (IACUC, #PROTO201901034). CDX models were established to test *in vivo* efficacy of CX+VEN combination as

described previously.[24] Further efficacy testing of this combination in a PDX model was described in the *Supplementary Appendix*. Kaplan–Meier analysis performed for estimating overall survival of xenograft mice.

Statistical analysis

Statistical tests were performed using GraphPad Prism 10.0 software. Results are presented as the means ± standard deviation (SD) or standard error of the mean (SEM) from at least two or three independent experiments. Comparisons between two groups were performed using a t-test, while three or more groups comparisons were evaluated by analysis of variance (ANOVA) with post hoc tests as provided in the respective figure legends. A p-value of less than 0.05 (95% CI) is considered statistically significant.

Results

High CK2 expression in AML correlates with poor survival and venetoclax resistance

Analysis of TCGA datasets revealed that AML patients with high *CSNK2A1* (CK2α) expression exhibit significantly decreased overall survival (OS) compared to those with low expression (**Figure 1A**). Specifically, elevated *CSNK2A1* levels correlate with poor-prognosis genetic subtypes, including those harboring *NPM1*, *SF3B1*, and *TP53* alterations (**Figure 1B**). TP53-mutated AML—which are strongly associated with VEN resistance—showed a significant correlation with high *CSNK2A1* levels (**Figure 1B**), suggesting that CK2 contributes to an adverse treatment response phenotype. To identify functional vulnerabilities and dependencies, we analyzed published genome-wide CRISPR screens in VEN-treated AML cell lines. Interestingly, CK2-deficient AML cells (targeted via *CSNK2A1* or *CSNK2B* sgRNAs) were significantly depleted in Molm13 and OCI-AML2 lines after 14 days of treatment (**Figure 1C**).[7,32] These changes are similar to known VEN-resistance mediators (BCL-XL and MCL1). These findings indicate a synthetic lethal relationship between CK2 and BCL2 inhibition.

To model VEN-resistant AML for further investigation, we characterized a panel of AML cell lines and patient-derived xenograft (PDX) cells from relapsed/refractory cases (**Figure S1A-B**). We chose two venetoclax-sensitive cell lines to generate acquired VEN-resistant cell models. MOLM13 is AML cell line with MLL-AF9 fusion, FLT3 internal tandem duplication and wild-type TP53. HL60 cell line harbors TP53 large deletion and c-Myc amplification. We generated acquired venetoclax-resistance (VR) models, Molm13-VR and HL60-VR by

exposing cells to increasing VEN doses for 8-12 weeks. VR cells exhibited IC_{50} greater than 1 μM (**Figure 1D**) and slower proliferation rates than parental lines (**Figure S1C**). These VR models also showed cross-resistance to standard AML frontline combination agents including decitabine, azacytidine, and cytarabine (**Figure S1D**). Molecular profiling of Molm13-VR cells revealed the upregulation of pro-survival BCL2-family members (*MCL1*, *BCL2L1*, *BCL2A1*) and the downregulation of pro-apoptotic *BAK* (**Figure S1E**). This is consistent with published results showing VEN-resistance in MOLM13 is characterized by decreased BCL2 dependency, increased reliance on MCL1 for survival, metabolic reprogramming, and activation of RAS/MAPK signaling.[33] Differential gene expression analysis by RNA-sequencing showed significant downregulation of genes involved in pro-apoptotic pathways (TNFα signaling, p53 pathway, apoptosis, STAT5 signaling) and upregulation of genes involved in heme metabolism that correlate with VEN resistance in Molm13-VR cells compared with parental Molm13 cells (**Figure S1F**). The differentially expressed genes (DEGs) and associated molecular gene signatures are comparable to those previously reported for the Molm13-VR transcriptome (GSE125403; **Figure S1F**).[34]

We used MOLM13 and MOLM13-VR as MCL1 driven VEN resistance model for further experiments. Results were validated in three other cell lines, HL60-VR, U937, and PDX 2016-7. U937 is an AML cell line with complex karyotype including MLL rearrangement and TP53 mutation, and is inherently resistant to multiple chemotherapy agents, including VEN. 2016-7 is a pediatric relapsed AML patient-derived cell line with MLL-AF9 fusion, wild-type TP53, and resistant to VEN (IC_{50} > 1μM).[35] Flow cytometric analysis further identified elevated surface expression of the drug-resistance markers CD47 and CD123 in PDX, VR-AML cells, and inherently VEN-resistant U937 cells (**Figure 1E, S1G**). Finally, immunoblotting confirmed that VR-AML cells exhibit higher CK2 activity, as evidenced by elevated phosphorylation of AKT (S129) and CK2 substrates (**Figure 1F, S1H**). MCL-1, BCL-XL and BCL2A1 were all increased in expression in VR cells compared to parental cells (**Figure 1G**). Collectively, these data demonstrate that elevated CK2 activity is associated with VEN resistance, establishing a rationale for using the CK2 inhibitor CX-4945 to re-sensitize AML cells to apoptosis.

CX-4945 and VEN combination synergistically enhances apoptosis in AML, including VEN-resistant cells

Based on the observed high CK2 activity in AML and known function of CK2 as global apoptosis suppressor in leukemia, we hypothesized that genetic and pharmacologic inhibition of CK2 would enhance VEN cytotoxicity in AML cells as well as induce apoptosis in VR-AML cells. While monotherapy with either CX-4945 or VEN showed minimal cytotoxicity, the combination therapy reduced cell viability across all tested lines (**Figure 2A)**. To quantify the interaction between CX-4945 and VEN, we calculated the combination index (CI) based on the Chou-Talalay method utilizing the CompuSyn software.[30] Low CI scores (<1) confirmed robust synergistic activity in most AML cell lines and PDX models (**Figure 2B and 2C**). Notably, the addition of CX-4945 sensitized both inherent and acquired VR-AML cells reducing the VEN IC_{50} and synergistic cytotoxicity. Similar enhancement of VEN-mediated cytotoxicity was observed in VR-AML PDX cells (**Figure 2A-C**). This synergy was further evidenced by a significant increase in Annexin V-positive apoptotic populations in the combination group compared to monotherapy (**Figure 3A and 3B, S2A**). Furthermore, CX-4945/VEN combination treatment effectively downregulated the chemoresistance marker CD47 on the surface of VR-AML cells (**Figure 3C and 3D, S2B**).

To genetically validate these findings, we performed shRNA-mediated knockdown of the CK2 catalytic subunit isoforms (α and α') in Molm13-VR cells (**Figure S2C and S2D**). Genetic depletion of *CSNK2A1* and *CSNK2A2* partially restored VEN sensitivity, resulting in increased apoptotic activity compared with non-targeting controls (**Figure S2E**). CX-4945 also showed synergistic cytotoxicity with decitabine, 5-Azacytidine, and cytarabine across multiple cell lines (**Figure S3**). Given that, VEN is rarely used clinically as a single agent, and VEN-based therapy includes hypomethylating agents (decitabine, 5-Azacytidine) or cytarabine, CX-4945 synergy with multiple agents is a significant advantage. Taken together, these results demonstrate that pharmacological inhibition of CK2 via CX-4945 potentiates VEN activity, driving synergistic cell death in AML, including VR-AML.

The CX-4945 and VEN combination targets MCL-1 to trigger apoptosis in AML

Recently, BH3 profiling assay has been proven to be a valuable functional biomarker for predicting clinical response and resistance towards BH3 mimetics.[36] So, we used BH3 profiling as a functional diagnostic tool to measure the apoptotic threshold, as indicated by mitochondrial priming and by the dependence of the parental

and VR-AML cells on specific BH3-family anti-apoptotic proteins. BH3 mimetic resistance is characterized by decreased mitochondrial outer membrane permeabilization (MOMP) as detected by the level of cytochrome c (Cyt C) release in the presence of BH3 peptide priming (**Figure 4A**). As expected, Molm13-VR cells showed reduced apoptotic priming compared with their parental Molm13 cells (**Figure 4B**). To gain functional insight and assess real-time changes in mitochondrial apoptotic signaling with CX-4945 and VEN combination, we performed dynamic BH3 profiling (**Figure 4C**). Exposure to CX-4945 enhanced the apoptotic priming of BH3 peptides, significantly increasing Cyt C release in both parental Molm13 and Molm13-VR cells (**Figure 4D**). These data suggest that CK2 inhibition overcomes BCL-2 antagonist resistance by increasing overall apoptosis sensitivity, effectively bypassing the cellular dependence on alternative anti-apoptotic BCL-2 family members.

MCL1 is a pivotal anti-apoptotic BCL-2 family member that serves as a primary determinant of resistance to BCL-2 targeted therapies.[37] MCL1 expression is significantly higher in VR cells compared to parental cells (**Figure 1G**). Beyond the full-length anti-apoptotic MCL-1L (L-long) isoform, alternative RNA splicing generates pro-apoptotic isoforms, such as MCL-1S (S-short) and MCL-1ES (ES-extra-short). These truncated variants antagonize MCL-1L and facilitate mitochondrial depolarization, often in a BAX/BAK-independent manner.[37] Post-translational caspase-mediated cleavage of MCL1 isoforms also generates shorter MCL1 fragments, some of which have pro-apoptotic activity.[38-40] The red arrow in **Figure 5** points to the shortest MCL1 fragment that represents a readout of apoptosis triggered by drug exposure.

To evaluate biochemical synergy between CX-4945 and venetoclax, we measured MCL1 protein levels following treatment with either drug alone or in combination (**Figure 5A, S4A**). In the control cells, we note three distinct bands representing different MCL1 isoforms. Exposure to venetoclax alone triggered several changes, including a significant increase in all three MCL1 isoforms and a 4th band (red arrow) that represents an apoptosis-induced MCL1 cleavage fragment (~20 kDa, denoted as MCL1Δ) (**Figure 5A, S4A**). However, this low-level proteolysis fails to trigger widespread apoptosis, as high MCL1 levels effectively prevent apoptosis and maintain the survival threshold. Treatment with CX-4945 alone significantly decreased anti-apoptotic MCL1L levels with no/minimal levels of cleavage fragment. At this stage, following CX-4945 single agent exposure, AML cells survive, but their total MCL1 pool is depleted, lowering their apoptotic threshold (priming the cell for

apoptosis), as reflected in the BH3 profiling (**Figure 4**). Finally, the CX+VEN combination increased apoptosis, and an increased, prominent MCL1 cleavage fragment at ~20 kDa (**Figure 5A**). These changes were observed across several cell lines tested including the VR cells and PDX cells (**Figure 5A, and S4A**). We noted that the shorter MCL1 fragment almost disappeared under pan-caspase blockade with z-VAD-FMK (**Figure 5B**), confirming that the short MCL1 fragment is a readout of apoptosis (**Figure 5B, 5C**). Since z-VAD-FMK pre-treatment failed to restore MCL1L levels after CX-4945 treatment for 6h (**Figure 5B**), we reasoned to test MCL1 post-translational regulation other than caspase-mediated cleavage. Our immunoblotting analysis showed that MCL1L protein levels begin to decline as early as 2 hours post-treatment with CX-4945 (**Figure 5D**). We further confirmed that in the CX-4945 single-agent arm at 2 hours, MCL-1L reduction is apparent while cleaved caspase-3 is undetectable. This demonstrates that MCL-1L loss precedes apoptotic execution (**Figure 5D** and **S4B-C**). This early decrease in MCL1 occurs before transcriptional shifts, suggesting a post-translational mechanism. We investigated whether CK2 inhibition accelerates proteasome-mediated protein degradation, driving the early decrease in full-length MCL-1L. Proteasome inhibitor MG132 co-treatment rescued full-length MCL-1L levels following CX-4945 exposure (**Figure 5D** and **S4C**). These findings are consistent with CX-4945 mediated promotion of proteasomal degradation of MCL-1. Overall, CX+VEN decisively shifted cells toward a pro-apoptotic state (**Figure 4** and **5**).

CX-4945 reduces MCL1 while minimally altering BCL-XL protein in most cell lines (MOLM13, HL60, 2016-7) (**Figure 5A**, **S4A**), suggesting that MCL1 reduction is the primary driver of venetoclax sensitization. Because venetoclax sensitizes these cells despite BCL-XL remaining high, BCL-XL is unlikely to be the major anti-apoptotic protein blocking venetoclax activity in these cell lines. These findings support MCL1 downregulation as the major contributor to the noted synergy in these cell lines. Further functional validation is needed to confirm these findings across AML cell panel. Next, we observed a consistent decrease in CK2 activity, as indicated by reduced substrate phosphorylation with CX-4945 alone and in VEN combination treatment (**Figure 5E**, **S4D**).

Because CK2-mediated signaling via the AKT/mTOR axis regulates MCL-1 at both the transcriptional and translational levels, we utilized qPCR and immunoblotting to assess MCL-1 expression and isoform

dynamics following CX-4945 and VEN combination treatment. Combination treatment induced minimal MCL-1 mRNA suppression after 24 hours treatment, which was variable across the cell lines tested, with the most significant decrease noted in the Molm13 and PDX cells (**Figure S4E**). Collectively, our findings are consistent with CX-4945 and VEN cooperatively suppressing CK2 activity and depleting pro-survival MCL1 protein via accelerated proteasome-mediated protein degradation. CX-4945 prevented the adaptive upsurge of MCL1 to stop AML cells from shifting into a state of MCL1 dependency (**Figure 5A**).

CK2 on-target specificity of CX-4945 – Given that CX-4945 is a potent multi-kinase clinical candidate that targets CLKs, DYRKs, and PIM kinases at low thresholds alongside CK2, we used a highly selective CK2 inhibitor SGC-CK2-1 to recapitulate the anti-proliferative and venetoclax-sensitizing effects in AML cells. SGC-CK2-1 is a chemical probe designed by the Structural Genomics Consortium to specifically target the catalytic subunit of CK2 (*CSNK2A1*), leaving the CLK /splicing machinery unaltered.[41] Our results show that SGC-CK2-1 mirrors the venetoclax-sensitizing and anti-proliferative phenotype of CX-4945 in AML cells (**Figure S5**). This supports the conclusion that the therapeutic synergy of CX-4945 and VEN in AML is an 'on-target' effect of CK2 inhibition.

The CX-4945 and VEN combination rewires apoptotic and survival transcriptomes in resistant AML

To elucidate the transcriptional landscape underlying BCL-2 and CK2 co-inhibition, we performed RNA-Sequencing on Molm13-VR cells following 24 h of treatment with CX-4945, VEN, or the combination. Principal component analysis (PCA) revealed significant transcriptional variability induced by the treatments, with 2731, 2327, and 3763 genes differentially regulated at least 1.5-fold (adjusted $p<0.05$) by CX, VEN, and the combination, respectively (**Figure S6A and S6B**). Hierarchical clustering identified six distinct gene clusters (**Figure 6A**). Notably, Cluster 4 was enriched for apoptosis, p53 signaling, and cell cycle checkpoint genes, all of which were upregulated by the combination treatment. Conversely, Clusters 5 and 6 contained genes involved in mTOR signaling, the unfolded protein response (UPR), and hypoxia, which were significantly repressed by CX and the combination (**Figure 6B**). The Molecular Signatures Database (MSigDB) hallmark gene set enrichment analysis confirmed that pro-apoptotic signatures (e.g., TNFα signaling, p53 pathway, and E2F targets) were restored following combination treatment, reversing the suppression observed in the Molm13-VR

phenotype (**Figure S6C and S6D**). Importantly, the combination treatment downregulated heme metabolism, a signature previously shown to correlate with VEN resistance.[42] Additionally, pro-survival pathways, including mTORC1 signaling, hypoxia, Myc targets, and glycolysis, were significantly suppressed (**Figure S6C)**.

We extended this transcriptomic profiling to PDX 2016-7 cells to validate these mechanisms in an inherently VEN-resistant patient-derived model. While VEN monotherapy failed to induce significant transcriptomic shifts, CX and the combination treatment profoundly altered the transcriptome, affecting 912 and 1018 genes, respectively (**Figure S6A** and **S6E**). Cluster analysis identified five groups; Clusters 1 and 2, which included genes for oxidative phosphorylation, UPR, and mTOR signaling, were markedly downregulated by the combination (**Figure 6C, 6D** and **S6F**). Functional enrichment revealed the upregulation of TNFα signaling via NF-κB and interferon responses, alongside the downregulation of mTORC1 and STAT5 signaling (**Figure S6G**). Importantly, the combination treatment reversed the expression of genes typically elevated in VEN non-responders,[43] P53 targets and upregulated pro-apoptotic BCL-2 family members (**Figure 6E**). Given that both Molm13-VR and PDX 2016-7 models harbor MLL-rearrangements (MLL-r), we assessed MLL-r specific gene signatures. CX and the combination differentially regulated genes involved in cell morphology, migration, and immune defense (**Figure S7A-D**). Finally, DrugSeq (drug perturbation) analysis indicated that the transcriptional response to the CX+VEN combination mimics that of established eIF4A3, PI3K/mTOR, and multi-tyrosine kinase inhibitors (**Figure S7E-H**). Collectively, these global transcriptomic data provide a mechanistic basis for how CX-4945 acts as a single agent and in synergy with VEN to bypass apoptotic blocks and inhibit multiple survival axes in VEN-resistant AML.

The CX-4945 and VEN combination induce apoptosis in primary AML cells

To validate the clinical relevance of our findings, we evaluated the efficacy of the CX-VEN combination in primary AML patient samples. Genetic profiling revealed a diverse cohort, including FLT3, MLL-r, and IDH mutations, alongside samples without unfavorable cytogenetics (**Table S2**). Consistent with our previous results, cells harboring FLT3 or MLL mutations exhibited elevated CK2α expression and increased substrate phosphorylation compared to AML without unfavorable cytogenetics and healthy donor PBMCs (**Figure S8A**). Additionally, several primary AML samples demonstrated high basal levels of the anti-apoptotic mediator BCL-XL (**Figure**

S8A). Samples with low basal apoptotic activity were selected for *ex vivo* drug sensitivity assays (**Figure S8B**). Baseline surface markers in the selected primary samples showed very low (<2%) CD34+ CD38- subpopulation (**Figure S8C**). We tested apoptotic response using the six primary AML patient samples following treatment with CX, VEN or combination (**Figure S8D**). The combination effect was pronounced in the two cases harboring FLT3-ITD mutations (674, 494) coupled with high CK2 substrate activity (**Figure S8A**, **S8D**). Conversely, samples with normal cytogenetics (9215, 9192) showed high baseline sensitivity to single-agent CX-4945, making an additive combination effect less evident. These patient-specific data suggest that specific venetoclax-resistant AML molecular subgroups—specifically FLT3-ITD AML with elevated CK2 substrate activity are likely to benefit from this rational therapeutic combination. However, due to limitations in the availability and quality of primary AML samples representing various genetic subgroups, further large-scale studies are needed to confirm these findings and the underlying mechanism. Next, we assessed the impact of the combination on specific high-risk subpopulations. In AML, the CD47+ population represents a subset of leukemic cells that is enriched for leukemia stem cells and drives chemoresistance.[44] In primary AML cells co-stained for CD47 and Annexin-V, we observed selective apoptotic targeting of phenotypically defined CD47 surface marker-positive AML cells after treatment with CX and VEN combination (**Figure S8E, S8F**). However, functional validation is required to confirm the eradication of true leukemia stem cells. Collectively, these data demonstrate that the CX-4945/VEN combination is effective in primary AML patient samples representing various molecular subtypes.

The CX-4945 and VEN combination is safe and synergistically prolongs survival in AML xenograft models

To evaluate the translational potential of our findings, we assessed the *in vivo* anti-leukemia effect of the CX-4945 and VEN combination across multiple VEN-resistant AML preclinical models, including acquired-resistance (Molm13-VR), inherently resistant (U937), and patient-derived xenograft (PDX 2016-7) models (**Figure 7A**). We evaluated the therapeutic efficacy of combination treatment using a multi-tiered approach that monitors not only leukemia burden, survival outcomes, and molecular target inhibition. Notably, the combination was well tolerated across all xenograft models tested; toxicological assessment showed no evidence of weight loss or exacerbated myelosuppression compared with VEN monotherapy (**Figure S9**). Specifically, no significant decrease in platelet count was noted in mice receiving CX-4945 alone or in combination with VEN (**Figure S9**). CX+VEN

synergistically prolonged median survival across all three AML xenograft models tested, the effect is most significant in the PDX model (**Figure 7B**). They all represent VEN-resistant preclinical models, and U937 represents TP53 mutant AML. The PDX mice receiving the CX+VEN combination achieved a significantly longer median survival (MS) of 41 days, compared with 30–34 days for monotherapies and 27 days for vehicle control (**Figure 7C**). Given the robust engraftment of leukemia cells and high baseline leukemia burden at treatment initiation, these xenografts appropriately modeled relapsed-refractory acute AML patients. While the high leukemic burden and abbreviated treatment window precluded significant shifts in BM infiltration, the CX+VEN combination effectively reduced AML cell infiltration in the spleen (**Figure S10A-D**). This was evidenced by reductions in spleen weight (**Figure S10A**), the percentage of human CD45-positive cells (**Figure S10B and S10C**). *In vivo* target inhibition was confirmed via immunoblotting of harvested AML cells from spleen, which showed reduced CK2 activity (decreased p-AKT S129) and a marked depletion of the anti-apoptotic mediator MCL1 in the combination group (**Figure 7D** and **7E**). This suggests that CK2 inhibitors can be used to inhibit MCL1 without causing off-target platelet toxicity, as seen with selective MCL1 inhibitors. Given that the VEN-resistant models represent aggressive AML (median survival of 4-weeks post-transplant), the modest survival benefit highlights the robust anti-tumor effect with co-targeting of CK2 and BCL-2.

Discussion

AML is a genetically and molecularly heterogeneous disease. Utilizing TCGA datasets, we found that elevated CK2α (*CSNK2A1*) levels correlate with poor survival. Furthermore, correlation analyses revealed that CK2 expression is significantly higher in AML patients with high-risk genetic alterations, including *TP53* and *WT1*. *TP53*-mutated AML patients have the worst outcome among all molecular subtypes.[45] Current venetoclax (VEN)-based combinations have failed to improve outcomes in TP53-mutated AML.[46] The evidence presented here supports the simultaneous targeting of BCL2 and the overactive protein kinase CK2 as a potential therapeutic strategy to enhance apoptosis in AML (**Figure 8**). We demonstrate synergy between CK2 inhibitor CX-4945 and VEN using multiple preclinical models of AML, including MLL-rearranged AML (MOLM13, MV4-11, THP-1, 2016-7 PDX), acquired VEN resistance model (Molm13-VR, HL60-VR), and a TP53-null/mutated (HL60 and HL60-VR, K562, THP-1, U937, 2016-1 PDX), complex karyotype multidrug resistant AML model (U937).

Rapid development of resistance to VEN-based therapy is multifactorial and characterized by diverse genetic alterations, including TP53 mutations, FLT3 activation, and BAX loss-of-function.[6-8] Beyond these mutations, the overexpression of anti-apoptotic proteins—specifically MCL1, BCL-XL, and BCL2A1—facilitates a shift away from BCL2 dependency, driving acquired resistance to VEN.[47] One established strategy to overcome VEN resistance is the dual blockade of MCL1 and BCL-XL.[9] Although we previously demonstrated that CX-4945 regulates BCL-XL levels via the CK2/IKAROS axis in high-risk B-ALL and AML, this effect was not consistent across the cell lines used.[21,24] Recently, CX-4945 was shown to potentiate VEN-mediated apoptosis in ALL and mantle cell lymphoma by downregulating MCL1.[48,49] Moreover, CK2 is ubiquitously expressed and is dysregulated in cancer, influencing key processes such as growth, metabolism, signaling, and chemoresistance.[50,51] Therefore, we hypothesized that adding CX-4945, which targets multiple survival and evasion pathways, represents a promising combination strategy to enhance the anti-leukemia activity of the VEN-based regimen. Evidence of synergy across multiple AML models reinforce broad applicability of this combination therapy (CX-4945 + VEN-based regimen) for treating AML with diverse genetic backgrounds and sensitivity profiles.

By analyzing genome-wide CRISPR loss-of-function screens, we identified that CK2-coding genes (*CSNK2A1, CSNK2B*) were negatively selected, indicating that their loss synergizes with VEN. We further observed that VR-AML cell lines exhibit elevated CK2 expression and activity. CX-4945 sensitized AML cell lines and patient-derived xenograft (PDX) cells to VEN, reducing IC50 values. Notably, the CX-4945/VEN combination induced synergistic apoptosis across genetically diverse AML cell lines and primary patient samples, reinforcing CK2 inhibition as a strategy to induce apoptosis in various AML genetic subtypes as well as the VEN-resistant AML.

Venetoclax is used in combination with hypomethylating agents (5-Azacytidine, decitabine) and low-dose cytarabine, and we have shown that CX-4945 synergizes with these agents. These findings support the addition of CK2 inhibitor to VEN backbone therapy to suppress anti-apoptotic and cell survival signals and achieve sustained disease remission. Further studies to test the mechanism of synergy with cytarabine and hypomethylating agents are underway. CX-4945-venetoclax synergy operates via a TP53-independent mechanism, making it relevant for refractory AML regardless of p53 status. Given the importance of CK2 in TP53 regulation and the significant change in TP53 signature following CX-4945 noted here, future studies will focus

on evaluating CK2 inhibition in relevant TP53-mutated AML models. CX-4945 has documented to inhibit off-target kinases, such as CLKs (CDC-like kinases) and DYRKs (Dual specificity tyrosine-regulated kinases), at the micromolar concentrations used in AML cell lines. While off-target activities may account for the baseline cellular toxicity of CX-4945, the specific mechanism driving its synergy with venetoclax—namely, MCL1-dependent apoptotic priming—is largely via inhibition of the CK2 pathway.

Mechanistically, we showed that the primary direct effect of CX-4945 is the inhibition of CK2 kinase activity, confirmed by decrease in Akt phosphorylation at Ser129, an established biomarker of intracellular CK2 catalytic activity. Next, we observed downregulation of MCL1 protein levels starting as early as 2-6 hours post-treatment. At this early time point, no increase in apoptosis and no caspase activation were noted in CX-4945-treated cells. This rapid decrease in MCL1 occurs before transcriptional shifts, suggesting a post-translational mechanism, likely accelerated MCL1 proteasomal degradation. Loss of the anti-apoptotic gatekeeper MCL1 directly shifts the intracellular balance of BCL-2 family proteins, inducing mitochondrial apoptotic priming at 12-24 hours. Finally, apoptosis, indicated by Annexin V positivity as a secondary consequence of this primed state, was noted when combined with the BCL-2 inhibitor venetoclax.

In vivo, the CX-4945/VEN combination extended survival in mice xenografted with VR-AML cell lines (Molm13-VR, U937) and PDX cells. While common AML therapy toxicities include anemia and thrombocytopenia,[52] the addition of CX-4945 was well-tolerated without exacerbating myelosuppression. CX-4945 has shown favorable safety profile in several completed and ongoing Phase 1 and 2 clinical trials; gastrointestinal effects are the most frequent adverse events and are typically manageable with supportive care. While direct MCL1 inhibitors have faced challenges due to dose-limiting cardiotoxicity in clinical trials,[11] the CX-4945 and VEN combination showed no evidence of cardiotoxicity in our mouse models, offering a safer alternative for direct MCL1 targeting. Furthermore, the addition of CX-4945 to upfront VEN-based therapy not only enhanced VEN cytotoxicity but will also likely prevent or delay the development of anti-apoptotic escape mechanisms by suppressing apoptotic pathway proteins.

In summary, combining the CK2 inhibitor CX-4945 with VEN-based therapy offers an effective strategy to suppress AML progression, including in acquired and innate VEN-resistant settings.

References

1. Siegel RL, Kratzer TB, Giaquinto AN, Sung H, Jemal A. Cancer statistics, 2025. CA Cancer J Clin. 2025;75(1):10-45.
2. Shimony S, Stahl M, Stone RM. Acute myeloid leukemia: 2025 update on diagnosis, risk-stratification, and management. Am J Hematol. 2025;100(5):860-891.
3. Pan R, Hogdal LJ, Benito JM, et al. Selective BCL-2 inhibition by ABT-199 causes on-target cell death in acute myeloid leukemia. Cancer Discov. 2014;4(3):362-375.
4. Jonas BA, Pollyea DA. How we use venetoclax with hypomethylating agents for the treatment of newly diagnosed patients with acute myeloid leukemia. Leukemia. 2019;33(12):2795-2804.
5. Pratz KW, Jonas BA, Pullarkat V, et al. Long-term follow-up of VIALE-A: venetoclax and azacitidine in chemotherapy-ineligible untreated acute myeloid leukemia. Am J Hematol. 2024;99(4):615-624.
6. Sullivan GP, Flanagan L, Rodrigues DA, Chongaile TN. The path to venetoclax resistance is paved with mutations, metabolism, and more. Sci Transl Med. 2022;14(674):eabo6891.
7. Nechiporuk T, Kurtz SE, Nikolova O, et al. The TP53 apoptotic network is a primary mediator of resistance to BCL2 inhibition in AML cells. Cancer Discov. 2019;9(7):910-925.
8. Moujalled DM, Brown FC, Chua CC, et al. Acquired mutations in BAX confer resistance to BH3-mimetic therapy in acute myeloid leukemia. Blood. 2023;141(6):634-644.
9. Lin KH, Winter PS, Xie A, et al. Targeting MCL-1/BCL-XL forestalls the acquisition of resistance to ABT-199 in acute myeloid leukemia. Sci Rep. 2016;6:27696.
10. Zhang H, Nakauchi Y, Kohnke T, et al. Integrated analysis of patient samples identifies biomarkers for venetoclax efficacy and combination strategies in acute myeloid leukemia. Nat Cancer. 2020;1(8):826-839.
11. Gui W, Paral P, Dhamija B, et al. MCL1 modulates mTORC1 signaling to promote bioenergetics and tumorigenesis. Nat Commun. 2025;16(1):10841.
12. Schoenwaelder SM, Jarman KE, Gardiner EE, et al. Bcl-xL-inhibitory BH3 mimetics can induce a transient thrombocytopathy that undermines the hemostatic function of platelets. Blood. 2011;118(6):1663-1674.
13. Van Gils N, Denkers F, Smit L. Escape from treatment; the different faces of leukemic stem cells and therapy resistance in acute myeloid leukemia. Front Oncol. 2021;11:659253.
14. Litchfield DW. Protein kinase CK2: structure, regulation and role in cellular decisions of life and death. Biochem J. 2003;369(Pt 1):1-15.
15. Litchfield DW, Bosc DG, Canton DA, Saulnier RB, Vilk G, Zhang C. Functional specialization of CK2 isoforms and characterization of isoform-specific binding partners. Mol Cell Biochem. 2001;227(1-2):21-29.
16. Landesman-Bollag E, Belkina A, Hovey B, Connors E, Cox C, Seldin DC. Developmental and growth defects in mice with combined deficiency of CK2 catalytic genes. Mol Cell Biochem. 2011;356(1-2):227-231.
17. Rajaiah R, Daniyal M, Shanmugam MP, et al. CK2alpha deletion in the hematopoietic compartment shows a mild alteration in terminally differentiated cells and the expansion of stem cells. Cells. 2025;14(13):963.
18. Meggio F, Pinna LA. One-thousand-and-one substrates of protein kinase CK2? FASEB J. 2003;17(3):349-368.
19. Di Maira G, Salvi M, Arrigoni G, et al. Protein kinase CK2 phosphorylates and upregulates Akt/PKB. Cell Death Differ. 2005;12(6):668-677.
20. Kalathur M, Toso A, Chen J, et al. A chemogenomic screening identifies CK2 as a target for pro-senescence therapy in PTEN-deficient tumours. Nat Commun. 2015;6:7227.
21. Song C, Ge Z, Ding Y, et al. IKAROS and CK2 regulate expression of BCL-XL and chemosensitivity in high-risk B-cell acute lymphoblastic leukemia. Blood. 2020;136(13):1520-1534.

22. Piazza F, Manni S, Ruzzene M, Pinna LA, Gurrieri C, Semenzato G. Protein kinase CK2 in hematologic malignancies: reliance on a pivotal cell survival regulator by oncogenic signaling pathways. Leukemia. 2012;26(6):1174-1179.
23. Quotti Tubi L, Canovas Nunes S, Brancalion A, et al. Protein kinase CK2 regulates AKT, NF-κB and STAT3 activation, stem cell viability and proliferation in acute myeloid leukemia. Leukemia. 2017;31(2):292-300.
24. Klink M, Rahman MA, Song C, et al. Mechanistic basis for in vivo therapeutic efficacy of CK2 inhibitor CX-4945 in acute myeloid leukemia. Cancers (Basel). 2021;13(5):1127.
25. Ning Y, Wang C, Liu X, et al. CK2-mediated CCDC106 phosphorylation is required for p53 degradation in cancer progression. J Exp Clin Cancer Res. 2019;38(1):131.
26. Schuster N, Prowald A, Schneider E, Scheidtmann KH, Montenarh M. Regulation of p53 mediated transactivation by the beta-subunit of protein kinase CK2. FEBS Lett. 1999;447(2-3):160-166.
27. Allende-Vega N, Dias S, Milne D, Meek D. Phosphorylation of the acidic domain of Mdm2 by protein kinase CK2. Mol Cell Biochem. 2005;274(1-2):85-90.
28. Borad MJ, Bai LY, Richards D, et al. Silmitasertib plus gemcitabine and cisplatin first-line therapy in locally advanced/metastatic cholangiocarcinoma: a phase 1b/2 study. Hepatology. 2023;77(3):760-773.
29. D'Amore C, Borgo C, Sarno S, Salvi M. Role of CK2 inhibitor CX-4945 in anti-cancer combination therapy - potential clinical relevance. Cell Oncol (Dordr). 2020;43(6):1003-1016.
30. Chou TC, Talalay P. Quantitative analysis of dose-effect relationships: the combined effects of multiple drugs or enzyme inhibitors. Adv Enzyme Regul. 1984;22:27-55.
31. Olesinski EA, Bhatt S. Dynamic BH3 profiling method for rapid identification of active therapy in BH3 mimetics resistant xenograft mouse models. STAR Protoc. 2021;2(2):100461.
32. Eide CA, Kurtz SE, Kaempf A, et al. Clinical correlates of venetoclax-based combination sensitivities to augment acute myeloid leukemia therapy. Blood Cancer Discov. 2023;4(6):452-467.
33. Tambe M, Unterberger S, Kriegbaum MC, et al. Venetoclax triggers sublethal apoptotic signaling in venetoclax-resistant acute myeloid leukemia cells and induces vulnerability to PARP inhibition and azacitidine. Cell Death Dis. 2024;15(10):750.
34. Chen X, Glytsou C, Zhou H, et al. Targeting mitochondrial structure sensitizes acute myeloid leukemia to venetoclax treatment. Cancer Discov. 2019;9(7):890-909.
35. Wunderlich M, Chen J, Sexton C, et al. PDX models of relapsed pediatric AML preserve global gene expression patterns and reveal therapeutic targets. bioRxiv. 2022 Feb 01. doi: 10.1101/2022.01.31.478534. [preprint, not peer-reviewed].
36. Pacchiardi K, de Marcellus V, Huynh T, et al. Prospective feasibility of a minimal BH3 profiling assay in acute myeloid leukemia. Cytometry B Clin Cytom. 2025;108(1):86-94.
37. Sancho M, Leiva D, Lucendo E, Orzaez M. Understanding MCL1: from cellular function and regulation to pharmacological inhibition. FEBS J. 2022;289(20):6209-6234.
38. Herrant M, Jacquel A, Marchetti S, et al. Cleavage of Mcl-1 by caspases impaired its ability to counteract Bim-induced apoptosis. Oncogene. 2004;23(47):7863-7873.
39. Ryu Y, Hall CP, Reynolds CP, Kang MH. Caspase-dependent Mcl-1 cleavage and effect of Mcl-1 phosphorylation in ABT-737-induced apoptosis in human acute lymphoblastic leukemia cell lines. Exp Biol Med (Maywood). 2014;239(10):1390-1402.
40. Menoret E, Gomez-Bougie P, Surget S, et al. Mcl-1(128-350) fragment induces apoptosis through direct interaction with Bax. FEBS Lett. 2010;584(3):487-492.
41. Wells CI, Drewry DH, Pickett JE, et al. Development of a potent and selective chemical probe for the pleiotropic kinase CK2. Cell Chem Biol. 2021;28(4):546-558.e10.

42. Mohanty V, Baran N, Huang Y, et al. Transcriptional and phenotypic heterogeneity underpinning venetoclax resistance in AML. bioRxiv. 2024 Jan 30. doi: 10.1101/2024.01.27.577579. [preprint, not peer-reviewed].
43. Khasawneh A, Paran FJ, Maiti A, et al. Transcriptomic signature of resistance to decitabine/venetoclax in AML patients. Blood. 2024;144(Supplement 1):2766.
44. Majeti R, Chao MP, Alizadeh AA, et al. CD47 is an adverse prognostic factor and therapeutic antibody target on human acute myeloid leukemia stem cells. Cell. 2009;138(2):286-299.
45. DiNardo CD, Tiong IS, Quaglieri A, et al. Molecular patterns of response and treatment failure after frontline venetoclax combinations in older patients with AML. Blood. 2020;135(11):791-803.
46. Venugopal S, Shoukier M, Konopleva M, et al. Outcomes in patients with newly diagnosed TP53-mutated acute myeloid leukemia with or without venetoclax-based therapy. Cancer. 2021;127(19):3541-3551.
47. Bhatt S, Pioso MS, Olesinski EA, et al. Reduced mitochondrial apoptotic priming drives resistance to BH3 mimetics in acute myeloid leukemia. Cancer Cell. 2020;38(6):872-890.e6.
48. Thus YJ, De Rooij MFM, Swier N, et al. Inhibition of casein kinase 2 sensitizes mantle cell lymphoma to venetoclax through MCL-1 downregulation. Haematologica. 2023;108(3):797-810.
49. Lázaro-Navarro J, Pimentel-Gutiérrez HJ, Gauert A, et al. Inhibiting casein kinase 2 sensitizes acute lymphoblastic leukemia cells to venetoclax via MCL1 degradation. Blood Adv. 2021;5(24):5501-5506.
50. Firnau MB, Brieger A. CK2 and the hallmarks of cancer. Biomedicines. 2022;10(8):1987.
51. Borgo C, Ruzzene M. Role of protein kinase CK2 in antitumor drug resistance. J Exp Clin Cancer Res. 2019;38(1):287.
52. Kurtin S. Myeloid toxicity of cancer treatment. J Adv Pract Oncol. 2012;3(4):209.

Figure legends:

Figure 1: Characterization of CK2 expression and activity in AML and VEN resistance. A) Overall survival analysis of AML patients with low and high expression of *CSNK2A1* (probe ID: 212072_s_at) from TCGA data (AML vs normal; accessed from BloodSplot database at https://www.fobinf.com/). **B)** The forest plot depicts the median difference (95% confidence interval) of CK2α (*CSNK2A1*) expression in the presence or absence of known somatic mutations in the indicated gene calculated using Mann-Whitney tests. The gene mutations that are significantly ($p<0.05$) associated with increased *CSNK2A1* expression and VEN resistance in the BeatAML cohort are highlighted in a red box. **C)** Enrichment of individual sgRNAs for genes encoding CK2 catalytic subunit (*CSNK2A1*) and regulatory subunit (*CSNK2B*), BCL-XL (*BCL2L1*), *MCL1*, and *TP53* plotted as log-fold change over control cells following 14 days of treatment with 0.5-1μM VEN in a CRISPR drop-out screening (data adopted from [7,32]). Genes encoding BCL-XL, MCL1, and TP53 were used as known controls that alter VEN activity. Data are presented as Mean ± SEM (n=4-5 sgRNAs targeting each gene). **D)** Parental and VR-AML cell lines were treated with different concentrations of VEN for 48 h and assessed for cell viability using WST. **E)** The surface expression of chemoresistance markers (CD47 and CD123) on AML cell lines and PDX 2016-7 cells was analyzed using flow cytometry. **F and G**) The basal level CK2 activity (substrate phosphorylation including AKT-S129) and expression of BCL2 family members in parental and VR-AML cell lines was analyzed by western blotting (**F**). β-Actin levels were used as loading controls. The levels of BCL2 family proteins were quantified relative to β-Actin and normalized to parental control cells (**G**).

Figure 2: Synergistic cytotoxic activity of CX-4945 and VEN combination in AML cell lines and PDX cells*.* A) AML cell lines and AML PDX cells (2016-1, 2016-7) were treated with different concentrations of CX-4945 and VEN alone or in combination with indicated doses for 48 h. Cell viability was assessed using WST reagent and cell viability was calculated relative to vehicle-treated cells as 100%. **B and C)** Combination index (CI) plots presenting fractional inhibition (Fa) and CI values in different AML cell lines and PDX cells after 48 h treatment with VEN (0.1-10μM) in combination with one or two doses of CX (2.5-10μM). CI values of <1 (below the line) indicate synergism between CX-4945 and VEN combination.

Figure 3: CX-4945 and VEN combination augments apoptosis and decrease chemoresistant marker CD47 levels in VEN-resistant AML cells. A and B) AML cells were treated with CX-4945 and VEN alone or in combination for 24 h and stained with Annexin V/7AAD for analyzing apoptosis by flow cytometry. Relative apoptosis was calculated by normalizing to vehicle-treated control cells (**A**). The data are presented as mean ± SD (n=2-4). *p<0.05, **p<0.01, ***p<0.001, and ****p<0.0001 by one-way ANOVA (Holm-Sidak's multiple comparisons test). A representative density plots showing Annexin V levels in AML cells after the drug treatment (**B**). **C and D)** AML cell lines were treated with IC_{50} doses of CX-4945 and VEN alone or in combination for 24 h and the surface expression of chemoresistance markers (CD47 and CD123) was analyzed by flow cytometry. Bar graph showing the percent populations of hCD47 positive AML cells after drug treatment (**C**). The data are presented as mean ± SEM (n=3). *p<0.05, **p<0.01, and ****p<0.0001 by two-way ANOVA (Dunnett's multiple

comparisons test). A representative density plot shows hCD123 and hCD47 levels in VEN-resistant AML cells after the drug treatment (**D**).

Figure 4: The effect of CX-4945 and VEN combination treatment on mitochondrial priming in AML cells. A) Schematic presentation of AML cells profiling with BH3 peptides (activators: BIM, BID; and sensitizer: PUMA) for the assessment of cytochrome c (Cyt C) release. **B)** Molm13 and Molm13-VR cells were tested for Cyt C release by priming with BH3 peptides and calculated the delta priming. The data are presented as mean ± SD (n=3) and *p<0.05, **p<0.01, ***p<0.001, and ****p<0.0001 by two-way ANOVA (Sidak's multiple comparisons test). **C)** Schematic showing the workflow for dynamic BH3 profiling to measure drug-induced apoptotic priming of BH3 peptides in AML cells. The difference in Cyt C release (%) with and without drug treatment was presented as delta priming. '**A** & **C**' were created in BioRender. Behura, C. (2026) https://BioRender.com/1a9dsr9. **D)** Molm13 and Molm13-VR cells were tested for Cyt C release by priming with BH3 peptides with and without CX-4945 treatment and calculated the delta priming. Representative data from two independent experiments are presented. Alamethicin (Ala) was used as a positive control to induce mitochondrial outer membrane permeabilization and maximum Cyt C release.

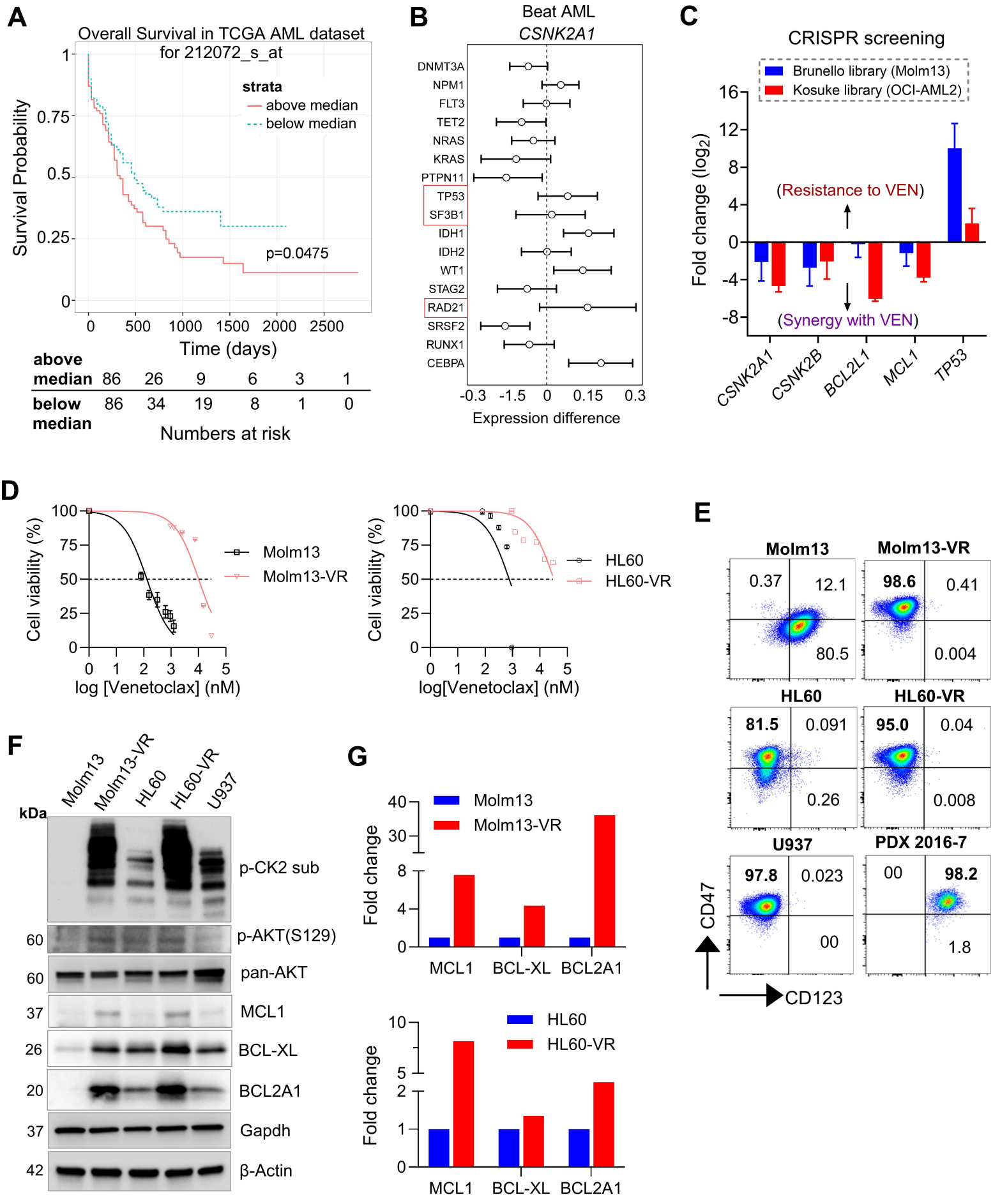
Figure 5: The effect of CX-4945 and VEN combination treatment on MCL1 levels in AML cells. A) Immunoblotting analysis of MCL1 and BCL-XL levels in AML cell lines (Molm13, Molm13-VR) and PDX (2016-1, 2016-7) cells after 24h of treatment with CX-4945 and VEN alone or in combination. The shortest band indicated by red arrow denotes proteolytic fragment of MCL1 protein (MCL1Δ). The levels of MCL1L (37 kDa) were quantified relative to β-Actin and normalized to vehicle control cells. **B)** Immunoblotting analysis of Molm13 AML cell lines after 6h of treatment with CX-4945 and VEN alone or in combination with or without z-VAD-FMK (50μM) pre-treatment for 2h. The shortest band indicated by red arrow denotes proteolytic fragment of MCL1 protein (MCL1Δ) by activated caspases. The levels of MCL1L were quantified relative to β-Actin and normalized to vehicle control cells. Blots from a representative experiment are shown '**A** & **B**'. **C)** Analysis of relative apoptosis (Annexin V) in Molm13 AML cells following 6h treatment with CX, VEN alone or in combination with or without z-VAD-FMK (50μM) pre-treatment for 2h. The data are presented as mean ± SD (n=2) and *p<0.05, **p<0.01, and ****p<0.0001 by two-way ANOVA (Sidak's multiple comparisons test). **D)** Immunoblotting analysis of Molm13 AML cell lines after 2h of treatment with CX-4945 in the presence or absence of proteasomal inhibitor MG132 (10 μM). The levels of MCL1L were quantified relative to Gapdh and normalized to vehicle (Veh) control cells. **E)** Immunoblotting analysis of AML cell lines (Molm13, Molm13-VR) after 24h of treatment with CX-4945 and VEN alone or in combination. β-Actin was used as a loading control and blots from a representative experiment are shown in '**D** & **E**'. 'cPARP' and 'cCaspase-3' denote cleaved PARP and cleaved Caspase-3, respectively in '**B** & **D**'.

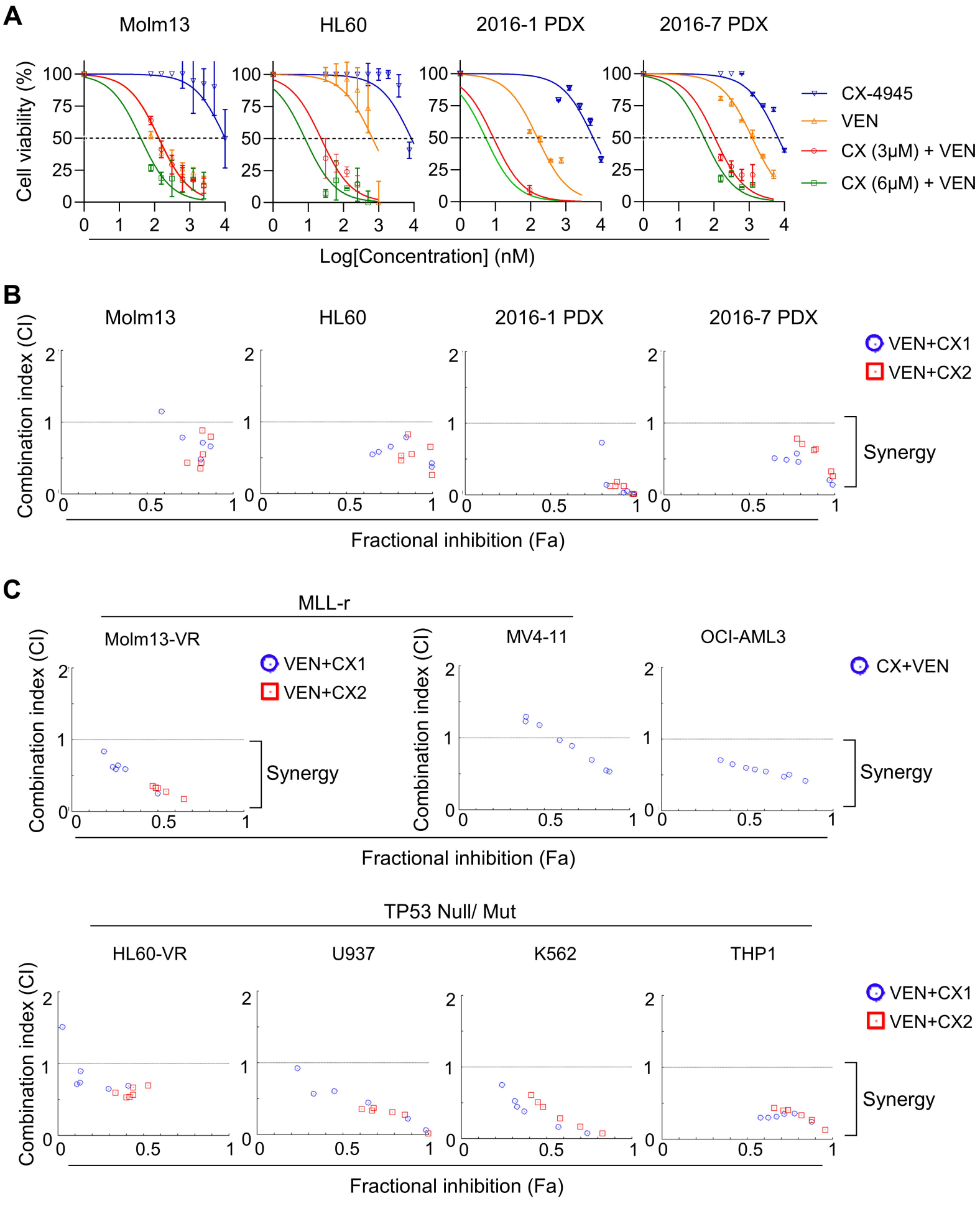
Figure 6: Differential gene expression and overrepresentation analysis with AML cells transcriptome after CX and VEN combination treatment. A) Heatmap showing the hierarchical clustering (k-means) of the most variable genes (n=2000) in Molm13 and Molm13-VR AML cell lines (24 h of drug treatment) transcriptome.

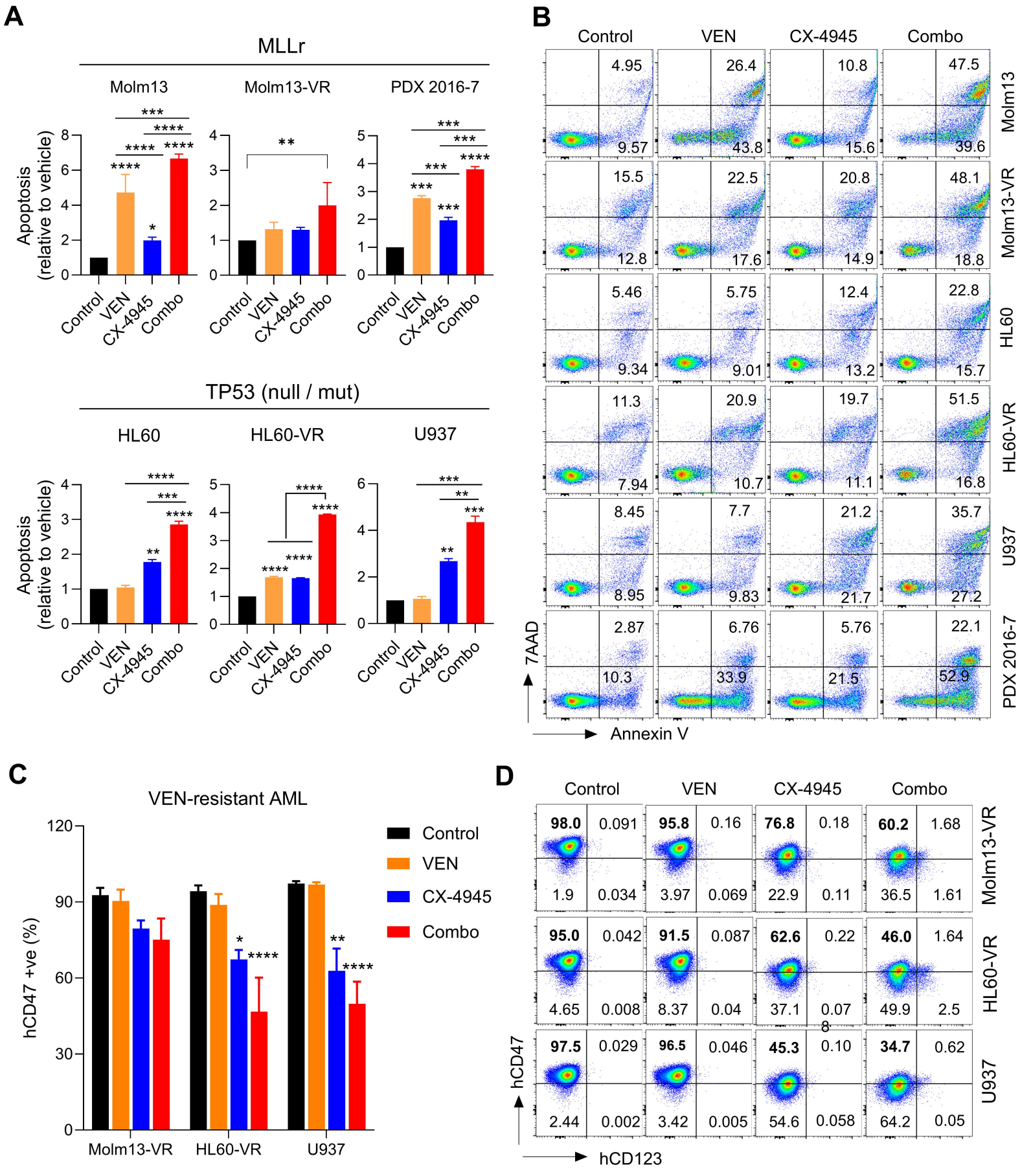
B) Dot plot displaying the top-ranked functional pathways (MSigDB hallmark gene set) overrepresented in different gene clusters obtained with k-means clustering as shown in '**A**'. **C)** Heatmap showing the hierarchical clustering (k-means) of most variable genes (n=2000) in PDX 2016-7 AML cells transcriptome after 24h of drug treatment. **D)** Dot plot displaying the top-ranked functional pathways (MSigDB hallmark gene set) overrepresented in different gene clusters obtained with k-means clustering as shown in '**C**'. **E)** Heatmap showing the expression profile of genes highly expressed in VEN non-responders (adapted from [43]), p53 target genes, and BCL2-family members (anti-apoptotic and pro-apoptotic) in PDX 2016-7 cells after 24h of treatment.

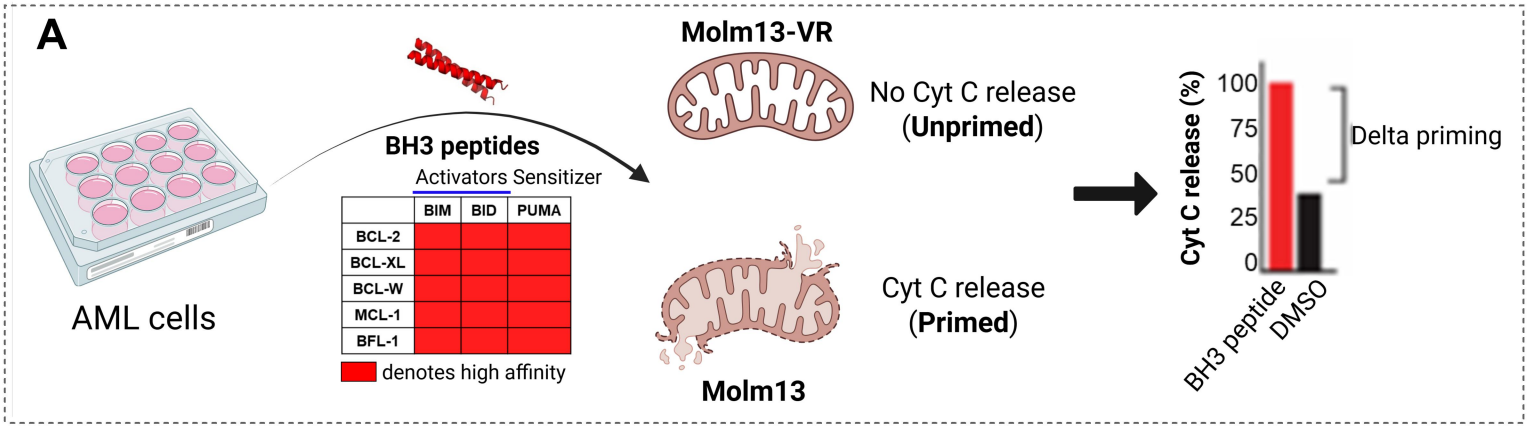
Figure 7: Anti-leukemic effect of CX-4945 in combination with VEN on AML-PDX, Molm13-VR and U937 cells xenograft in mice. A) Schematic depicting the treatment plan in AML patient-derived xenograft (PDX) mouse model. Similar scheme followed for cell line-derived xenograft (CDX) mice except the analysis after two weeks of treatment. The NRG-S mice were irradiated and intravenously injected with AML cell lines Molm13-VR ($0.25x10^6$ cells/mouse), U937 ($1x10^4$ cells/mouse), and PDX 2016-7 ($0.5x10^6$ cells/mouse) and randomized into experimental groups (Vehicle, CX-4945, VEN, and CX+VEN Como). The drug treatment started after one week of cell transplantation and followed up for survival analysis or analysis after two-weeks of treatment (only for PDX). **B and C)** Kaplan-Meier survival analysis of 2016-7 PDX, Molm13-VR CDX, and U937 CDX mice after treatment with CX-4945, VEN and CX+VEN combination (**B**). The overall median survival days for each experimental group of PDX and CDX mice were provided in the bar graph (**C**). *p<0.05, **p<0.01 and ***p<0.001 by Gehan-Breslow-Wilcoxon and log-rank tests indicate statistical significance. **D and E)** Immunoblotting analysis of spleen cells collected from PDX 2016-7 mice after two-weeks of treatment with CX-4945, VEN, and CX+VEN combination. The data for three different animals from each experimental group was presented (**D**). β-Actin levels were used as loading control. The MCL1 (human) levels were detected using two different antibodies. MCL1 and p-AKT (S129) levels were quantified relative to β-Actin and normalized to vehicle control group (**E**). The data are presented as mean ± SEM (n=3) and *p<0.05 by two-way ANOVA (Dunnett's multiple comparisons test).

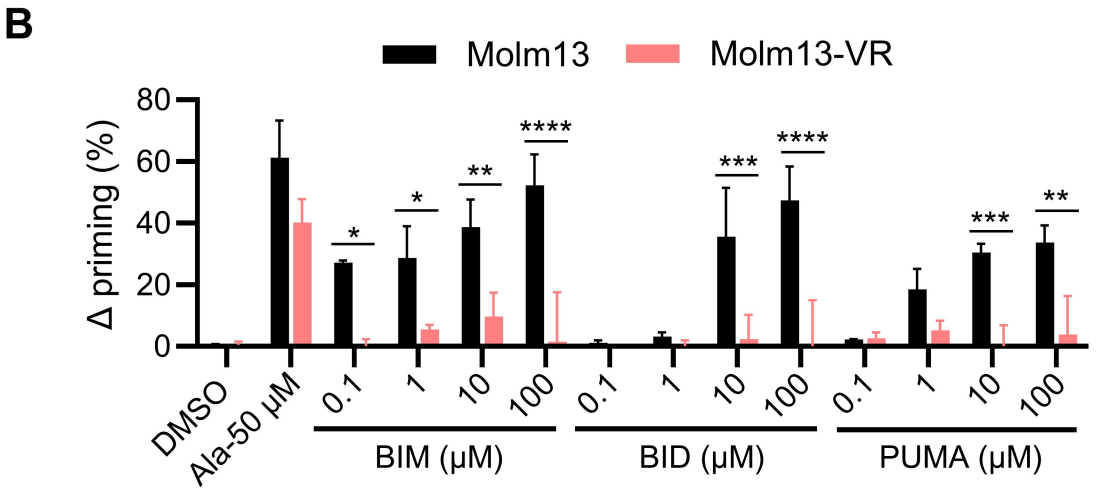
Figure 8: Summary model depicting the proposed mechanisms of action of CX-4945 and VEN combination in AML cells. The effectiveness of CK2 inhibitor CX-4945 in combination with VEN was tested in diverse pre-clinical AML models (*in vitro*, *ex vivo*, *in vivo*), including VEN-resistant AML cells. Mechanistically, inhibition of CK2-mediated signaling through CX-4945 negatively affects cell survival pathways (PI3K/AKT/mTOR, NF-κB pathways) and decrease in anti-apoptotic MCL-1L levels through post-translational regulation further increase BCL-2 dependency and enhances VEN-mediated apoptosis in VR-AML cells. Moreover, the transcriptome of VR-AML cells followed by CX-4945 and VEN combination treatment showed reversal of molecular gene signatures associated with VEN resistance and result in potentiated apoptosis in VR-AML cells. The signaling targeted by CX-4945 and VEN are represented by dotted lines in the working model. Created in BioRender. Behura, C. (2026) https://BioRender.com/4hnmtcz.

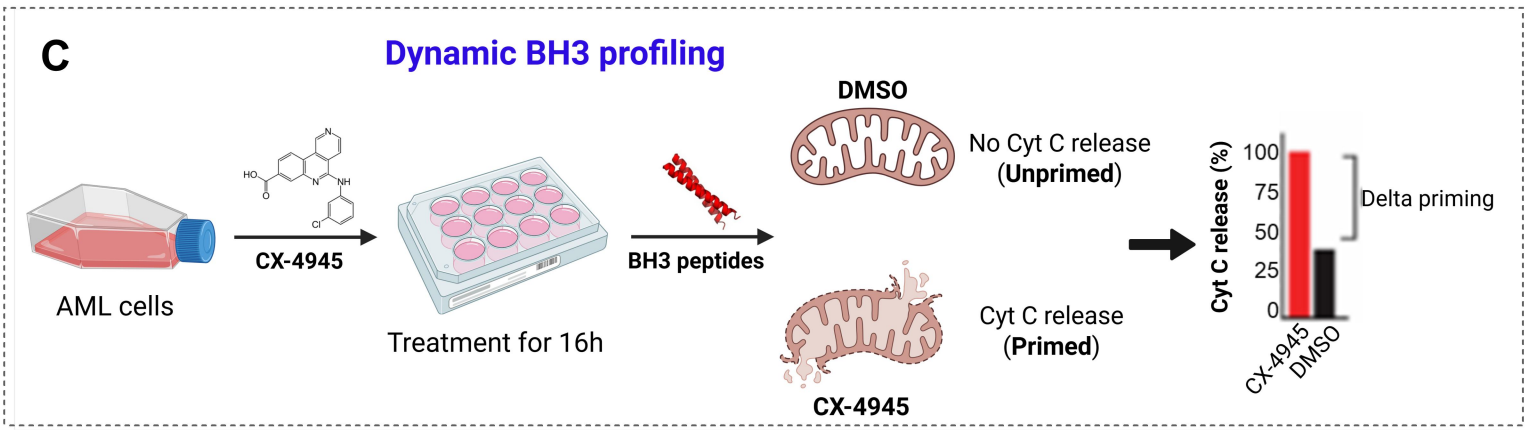

A
Overall Survival in TCGA AML dataset
for 212072_s_at
strata
above median
below median
p=0.0475
Survival Probability
Time (days)
above median 86 26 9 6 3 1
below median 86 34 19 8 1 0
Numbers at risk
B
Beat AML
CSNK2A1
DNMT3A
NPM1
FLT3
TET2
NRAS
KRAS
PTPN11
TP53
SF3B1
IDH1
IDH2
WT1
STAG2
RAD21
SRSF2
RUNX1
CEBPA
Expression difference
C
CRISPR screening
Brunello library (Molm13)
Kosuke library (OCI-AML2)
Fold change (log2)
(Resistance to VEN)
(Synergy with VEN)
CSNK2A1
CSNK2B
BCL2L1
MCL1
TP53
D
Cell viability (%)
Molm13
Molm13-VR
log [Venetoclax] (nM)
HL60
HL60-VR
log[Venetoclax] (nM)
E
Molm13
Molm13-VR
HL60
HL60-VR
U937
PDX 2016-7
CD47
CD123
F
Molm13
Molm13-VR
HL60
HL60-VR
U937
kDa
p-CK2 sub
p-AKT(S129)
pan-AKT
MCL1
BCL-XL
BCL2A1
Gapdh
β-Actin
G
Molm13
Molm13-VR
Fold change
MCL1
BCL-XL
BCL2A1
HL60
HL60-VR

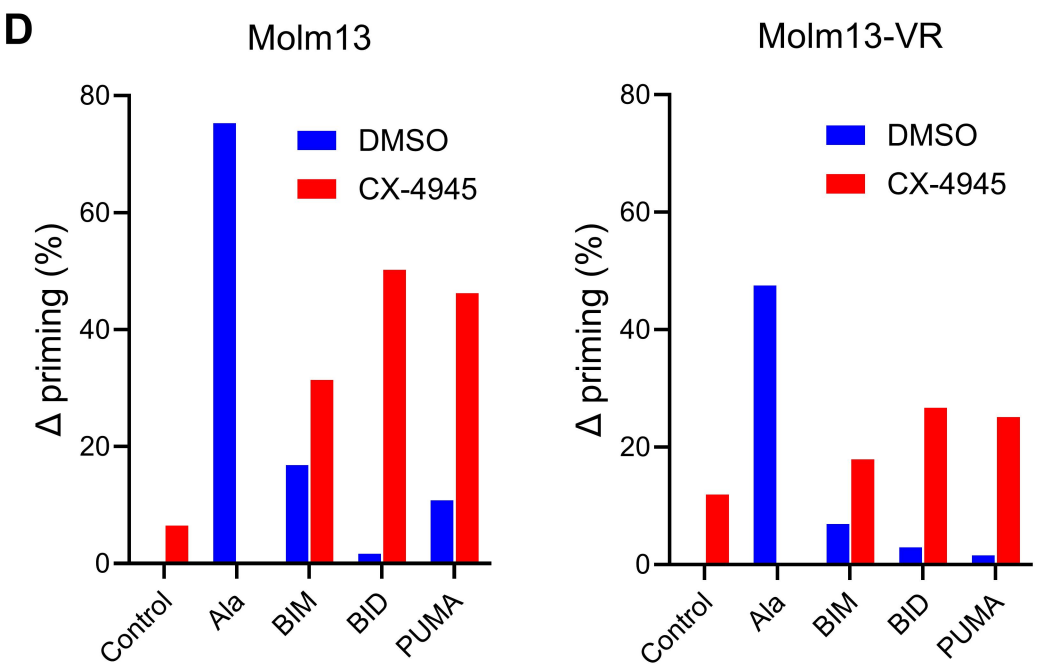

A
Molm13
HL60
2016-1 PDX
2016-7 PDX
Cell viability (%)
Log[Concentration] (nM)
CX-4945
VEN
CX (3μM) + VEN
CX (6μM) + VEN
B
Molm13
HL60
2016-1 PDX
2016-7 PDX
Combination index (CI)
Fractional inhibition (Fa)
VEN+CX1
VEN+CX2
Synergy
C
MLL-r
Molm13-VR
MV4-11
OCI-AML3
CX+VEN
TP53 Null/ Mut
HL60-VR
U937
K562
THP1

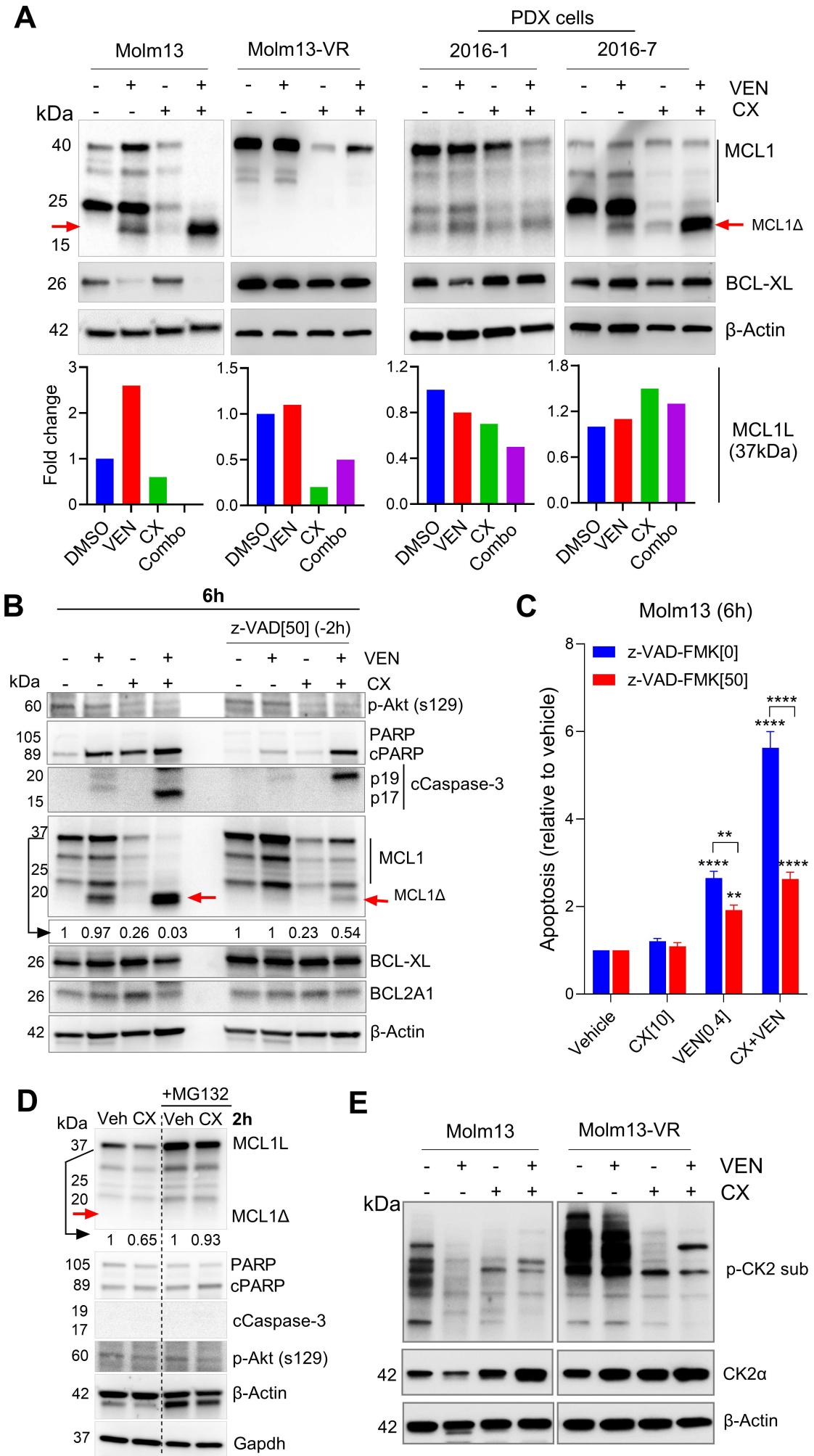

A
MLLr
Molm13
Molm13-VR
PDX 2016-7
Apoptosis (relative to vehicle)
Control
VEN
CX-4945
Combo
TP53 (null / mut)
HL60
HL60-VR
U937
B
Control
VEN
CX-4945
Combo
Molm13
Molm13-VR
HL60
HL60-VR
U937
PDX 2016-7
7AAD
Annexin V
4.95
26.4
10.8
47.5
9.57
43.8
15.6
39.6
15.5
22.5
20.8
48.1
12.8
17.6
14.9
18.8
5.46
5.75
12.4
22.8
9.34
9.01
13.2
15.7
11.3
20.9
19.7
51.5
7.94
10.7
11.1
16.8
8.45
7.7
21.2
35.7
8.95
9.83
21.7
27.2
2.87
6.76
5.76
22.1
10.3
33.9
21.5
52.9
C
VEN-resistant AML
hCD47 +ve (%)
Control
VEN
CX-4945
Combo
Molm13-VR
HL60-VR
U937
D
Control
VEN
CX-4945
Combo
Molm13-VR
HL60-VR
U937
hCD47
hCD123
98.0
0.091
1.9
0.034
95.8
0.16
3.97
0.069
76.8
0.18
22.9
0.11
60.2
1.68
36.5
1.61
95.0
0.042
4.65
0.008
91.5
0.087
8.37
0.04
62.6
0.22
37.1
0.078
46.0
1.64
49.9
2.5
97.5
0.029
2.44
0.002
96.5
0.046
3.42
0.005
45.3
0.10
54.6
0.058
34.7
0.62
64.2
0.05

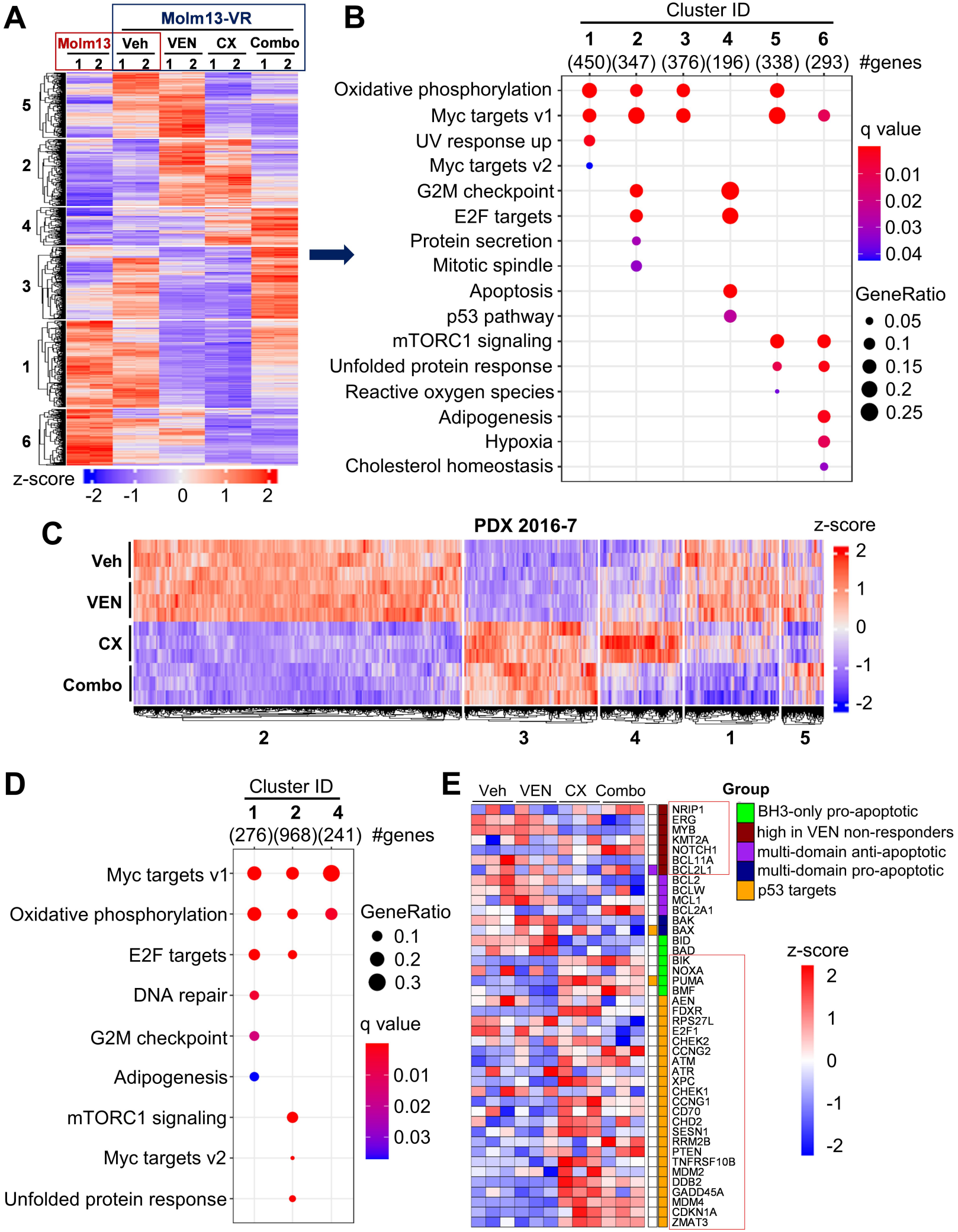

A
Molm13-VR
BH3 peptides
Activators Sensitizer
BIM
BID
PUMA
BCL-2
BCL-XL
BCL-W
MCL-1
BFL-1
denotes high affinity
AML cells
No Cyt C release
(Unprimed)
Cyt C release
(Primed)
Molm13
Cyt C release (%)
100
75
50
25
0
Delta priming
BH3 peptide
DMSO

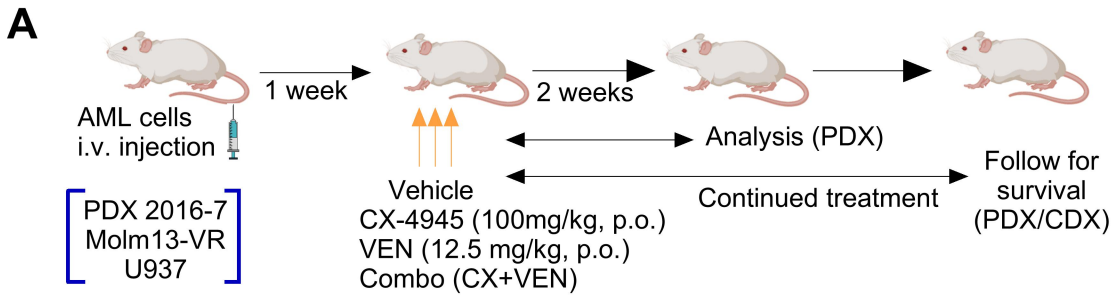

B
Molm13
Molm13-VR
Δ priming (%)
80
60
40
20
0
*
*
**
****
***
****
***
**
DMSO
Ala-50 μM
0.1
1
10
100
BIM (μM)
BID (μM)
PUMA (μM)

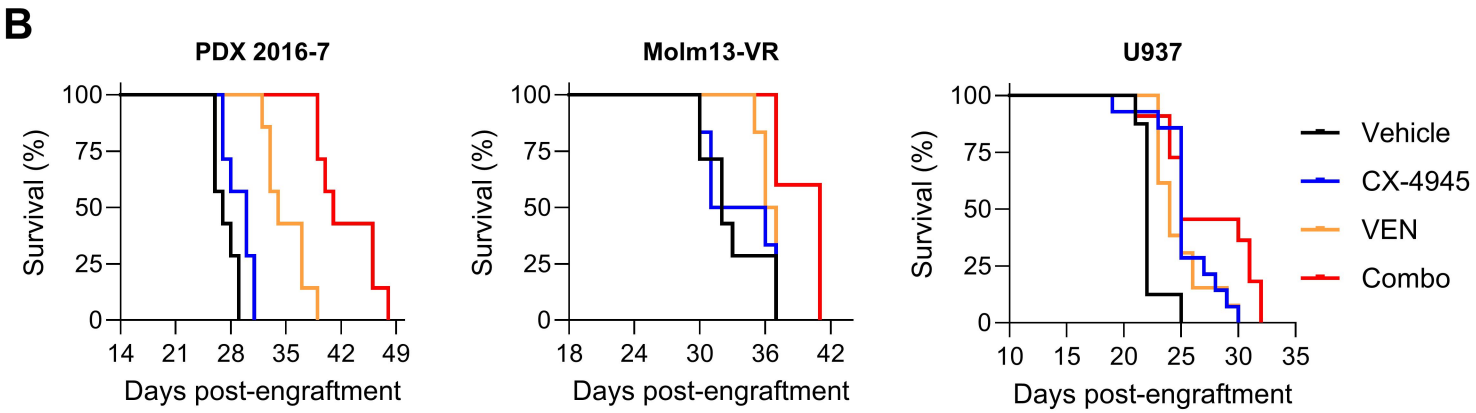

C
Dynamic BH3 profiling
AML cells
CX-4945
Treatment for 16h
BH3 peptides
DMSO
No Cyt C release
(Unprimed)
Cyt C release
(Primed)
CX-4945
Cyt C release (%)
100
75
50
25
0
Delta priming
CX-4945
DMSO

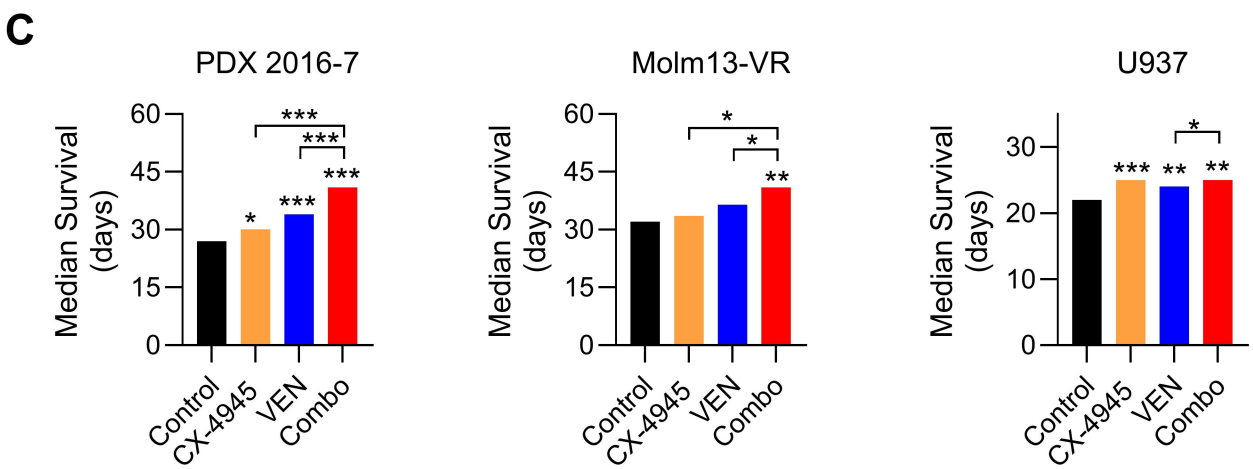

D
Molm13
Molm13-VR
DMSO
CX-4945
Δ priming (%)
80
60
40
20
0
Control
Ala
BIM
BID
PUMA

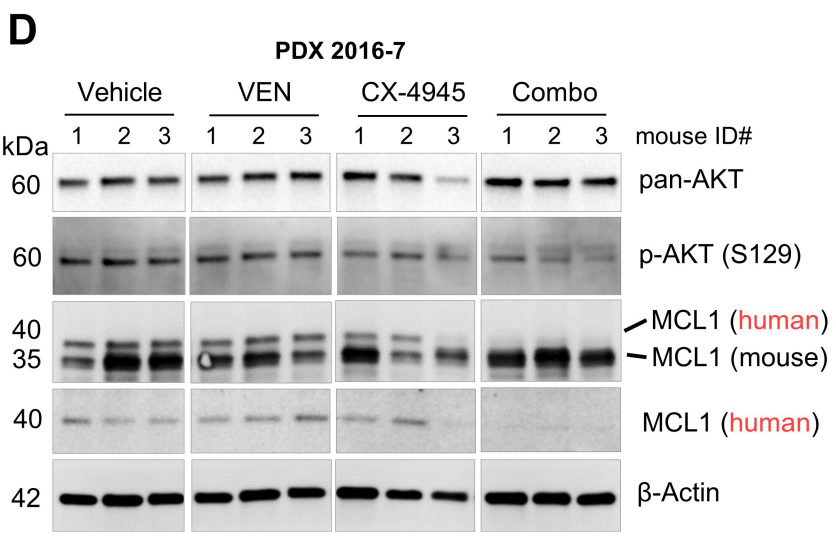

A
PDX cells
Molm13
Molm13-VR
2016-1
2016-7
VEN
CX
kDa
40
25
15
26
42
MCL1
MCL1Δ
BCL-XL
β-Actin
Fold change
MCL1L (37kDa)
DMSO
VEN
CX
Combo
B
6h
z-VAD[50] (-2h)
p-Akt (s129)
PARP
cPARP
p19
p17
cCaspase-3
MCL1
MCL1Δ
1 0.97 0.26 0.03 1 1 0.23 0.54
BCL-XL
BCL2A1
β-Actin
C
Molm13 (6h)
z-VAD-FMK[0]
z-VAD-FMK[50]
Apoptosis (relative to vehicle)
Vehicle
CX[10]
VEN[0.4]
CX+VEN
D
+MG132
Veh CX Veh CX 2h
MCL1L
MCL1Δ
1 0.65 1 0.93
PARP
cPARP
cCaspase-3
p-Akt (s129)
β-Actin
Gapdh
E
Molm13
Molm13-VR
p-CK2 sub
CK2α
β-Actin

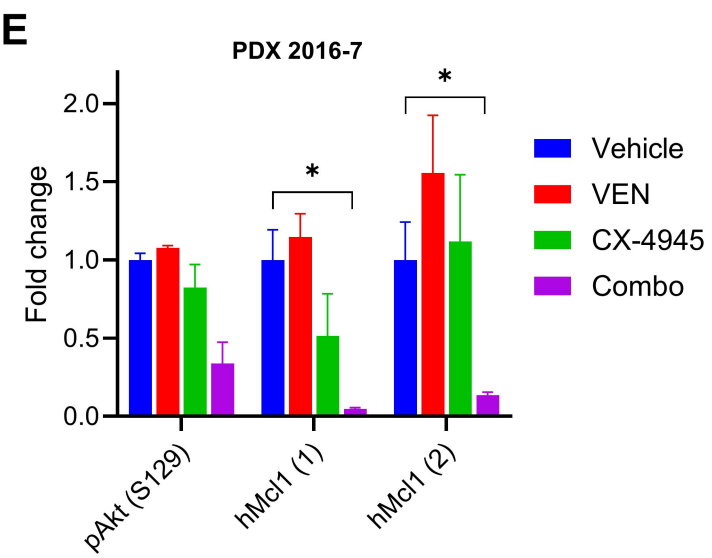

A
Molm13-VR
Molm13
Veh
VEN
CX
Combo
1 2
5
2
4
3
1
6
z-score
-2 -1 0 1 2
B
Cluster ID
1 2 3 4 5 6
(450)(347) (376)(196) (338) (293) #genes
Oxidative phosphorylation
Myc targets v1
UV response up
Myc targets v2
G2M checkpoint
E2F targets
Protein secretion
Mitotic spindle
Apoptosis
p53 pathway
mTORC1 signaling
Unfolded protein response
Reactive oxygen species
Adipogenesis
Hypoxia
Cholesterol homeostasis
q value
0.01
0.02
0.03
0.04
GeneRatio
0.05
0.1
0.15
0.2
0.25
C
PDX 2016-7
z-score
2
1
0
-1
-2
Veh
VEN
CX
Combo
2
3
4
1
5
D
Cluster ID
1 2 4
(276)(968)(241) #genes
Myc targets v1
Oxidative phosphorylation
E2F targets
DNA repair
G2M checkpoint
Adipogenesis
mTORC1 signaling
Myc targets v2
Unfolded protein response
GeneRatio
0.1
0.2
0.3
q value
0.01
0.02
0.03
E
Veh VEN CX Combo
Group
BH3-only pro-apoptotic
high in VEN non-responders
multi-domain anti-apoptotic
multi-domain pro-apoptotic
p53 targets
NRIP1
ERG
MYB
KMT2A
NOTCH1
BCL11A
BCL2L1
BCL2
BCLW
MCL1
BCL2A1
BAK
BAX
BID
BAD
BIK
NOXA
PUMA
BMF
AEN
FDXR
RPS27L
E2F1
CHEK2
CCNG2
ATM
ATR
XPC
CHEK1
CCNG1
CD70
CHD2
SESN1
RRM2B
PTEN
TNFRSF10B
MDM2
DDB2
GADD45A
MDM4
CDKN1A
ZMAT3
z-score
2
1
0
-1
-2

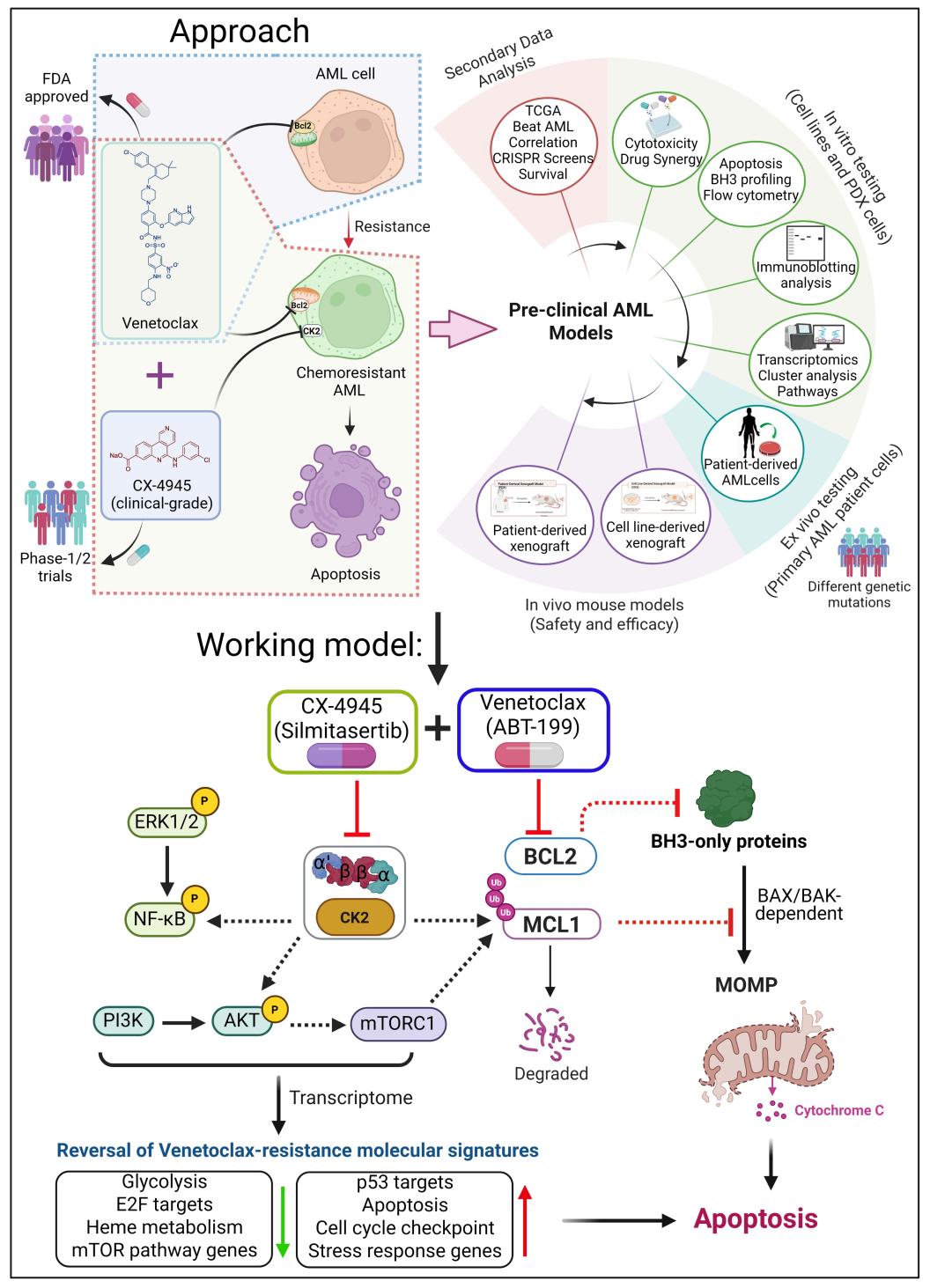

A
AML cells
i.v. injection
1 week
2 weeks
Analysis (PDX)
Follow for
survival
(PDX/CDX)
Continued treatment
PDX 2016-7
Molm13-VR
U937
Vehicle
CX-4945 (100mg/kg, p.o.)
VEN (12.5 mg/kg, p.o.)
Combo (CX+VEN)


B
PDX 2016-7
Molm13-VR
U937
Survival (%)
Days post-engraftment
Vehicle
CX-4945
VEN
Combo


C
PDX 2016-7
Molm13-VR
U937
Median Survival (days)
Control
CX-4945
VEN
Combo


D
PDX 2016-7
Vehicle
VEN
CX-4945
Combo
kDa
mouse ID#
pan-AKT
p-AKT (S129)
MCL1 (human)
MCL1 (mouse)
MCL1 (human)
β-Actin


E
PDX 2016-7
Fold change
Vehicle
VEN
CX-4945
Combo
pAkt (S129)
hMcl1 (1)
hMcl1 (2)


Approach
FDA approved
AML cell
Bcl2
Resistance
Venetoclax
Bcl2
CK2
Chemoresistant AML
CX-4945 (clinical-grade)
Phase-1/2 trials
Apoptosis
Secondary Data Analysis
TCGA
Beat AML
Correlation
CRISPR Screens
Survival
Cytotoxicity
Drug Synergy
Apoptosis
BH3 profiling
Flow cytometry
In vitro testing (Cell lines and PDX cells)
Immunoblotting analysis
Pre-clinical AML Models
Transcriptomics
Cluster analysis
Pathways
Patient-derived AMLcells
Patient-derived xenograft
Cell line-derived xenograft
Ex vivo testing (Primary AML patient cells)
Different genetic mutations
In vivo mouse models (Safety and efficacy)
Working model:
CX-4945 (Silmitasertib)
Venetoclax (ABT-199)
ERK1/2
NF-κB
CK2
BCL2
MCL1
BH3-only proteins
BAX/BAK-dependent
MOMP
PI3K
AKT
mTORC1
Degraded
Cytochrome C
Transcriptome
Reversal of Venetoclax-resistance molecular signatures
Glycolysis
E2F targets
Heme metabolism
mTOR pathway genes
p53 targets
Apoptosis
Cell cycle checkpoint
Stress response genes
Apoptosis

Supplementary Appendix:

Casein kinase II inhibitor CX-4945 synergizes with venetoclax to augment apoptosis by targeting MCL1 in both *in vitro* and *in vivo* models of venetoclax-resistant acute myeloid leukemia

Running title: Novel combination of CK2 inhibitor and venetoclax

Muhammad Daniyal[1#], Rajesh Rajaiah[1,a#], Upendarrao Golla[1], Marudhu Pandiyan Shanmugam[1], Morgann Klink[1,b], Koby Duke[1], Katherine Mercer[1,c], Preeti Bhadauria[1], Mohammad Atiqur Rahman[1,d], Soumya Iyer[1,e], Cesar Aliaga[2], Hannah Valensi[1], Jeremy Hengst[1,2], Yasin Uzun[2], Sinisa Dovat[1], Yi Qiu[3], Suming Huang[1], Chandrika G Behura[1*]

[1]Department of Pediatrics, Pennsylvania State University College of Medicine, Hershey, PA USA

[2]Department of Molecular and Precision Medicine, Pennsylvania State University College of Medicine, Hershey, PA USA

[3]Department of Cell and Biological Systems, Pennsylvania State University College of Medicine, Hershey, PA USA

[a]Present address: Center for Drug Evaluation and Research, Food and Drug Administration, Silver Spring, MD 20993, USA.

[b]Present address: AstraZaneca, Gaithersburg, MD 20878, USA.

[c]Present address: Maynard Children's Hospital at ECU Health Medical Center, Greenville, NC 27834, USA.

[d]Present address: Johnson & Johnson Innovative Medicine, Malvern, PA 19355, USA.

[e]Present address: University of Chicago, Chicago, IL 60637, USA.

[#]These authors contributed equally

***Corresponding Author:** Dr. Chandrika Gowda Behura

Email: cxg40@psu.edu; Fax: 717-531-4789

Methods

Drugs and Reagents

CX-4945 (#HY-50855B), SGC-CK2-1 (#HY-139004), Venetoclax (#HY-15531), 5-Azacytidine (#HY-10586), Decitabine (#HY-A0004), and Z-VAD-FMK (#HY-16658B) were purchased from MedChemExpress (Monmouth Junction, NJ). Cytarabine (#16069) was procured from Cayman Chemical (Ann Arbor, Michigan). Alamethicin (#BML-A150) was obtained from Enzo Life Sciences (Farmingdale, NY). Recombinant human cytokines including SCF (#100-04), GM-CSF (#100-08), and IL-3 (#100-80) were purchased from FUJIFILM Biosciences (Santa Ana, CA), whereas FLT-3 ligand (#PHC9411) and G-CSF (#PHC2031) were obtained from Thermo Fisher Scientific (Waltham, MA). All other reagents, antibodies, and chemicals were of molecular biology grade, and details are provided in the supplementary information.

Cell culture

Human AML cell lines U937 (#CRL-1593.2, RRID:CVCL_0007), HL60 (#CCL-240, RRID:CVCL_0002), THP-1 (#TIB-202, RRID:CVCL_0006), MV4-11 (#CRL-9591, RRID:CVCL_0064), and K562 (#CCL-243, RRID:CVCL_0004) were obtained from the American Type Culture Collection (ATCC), Molm13 (#ACC554, RRID:CVCL_2119) and OCI-AML3 (#ACC582, RRID:CVCL_1844) cells were purchased from the German Collection of Microorganisms and Cell Cultures (DSMZ). The characteristics of AML cell lines are provided in **Table S1**. All AML cell lines were cultured in RPMI-1640 (#10-040, Corning, NY) growth medium supplemented with 10% heat-inactivated fetal bovine serum (FBS) (#S11150; GeminiBio, West Sacramento, CA) and 1X Penicillin-Streptomycin (#15140122; Gibco, Gaithersburg, MD) at 37 °C in a humidified incubator with 5% CO_2. VEN-resistant (VR) derivatives of Molm13 and HL60 cell lines were generated by continued subculture with increasing doses of VEN (starting at IC_{50}) for 6-8 weeks. Cell lines were routinely confirmed to be negative for mycoplasma contamination and authenticated by short tandem repeat (STR) profiling (Promega, Madison, Wisconsin). Each cell line was propagated for no more than 30 passages after the initial thawing. Cell viability and counts were measured by trypan blue exclusion assay using CellDrop automated cell counter (DeNovix, Wilmington, DE).

Primary AML patient and patient-derived xenograft (PDX) AML cells

De-identified and clinically annotated human AML patient samples derived from either bone marrow or blood were obtained from the Institutional Biorepository Core (RRID:SCR_025728) at the Penn State College of Medicine in compliance with institutional review board (IRB #40532) regulations. Cryo-preserved patient-derived xenograft (PDX) AML cells were obtained from the collaborator and director of Developmental Therapeutic and Preclinical Core, Dr. Sinisa Dovat, who obtained samples from Cincinnati Children's Hospital after MTA. All primary and PDX AML cells were cultured in RPMI-1640 medium supplemented with 25% FBS, 1X penicillin/streptomycin, and 10 ng/mL of cytokines (IL-3, SCF, FLT-3, G-CSF, and GM-CSF) at 37 ^{o}C in a humidified incubator with 5% CO_2 as described earlier.[1] The clinical characteristics of the primary AML and PDX cells are summarized in **Tables S2 & S3**. Cell viability was measured via the trypan blue exclusion assay using CellDrop automated cell counter (DeNovix, Wilmington, DE).

Cell viability assays

The AML cell lines or PDX AML cells were seeded in 96-well flat-bottom plates at $1x10^5$ cells/mL in 0.1 mL/well and treated with increasing concentrations of CX-4945 (2-10 μM) in combination with either VEN (0.03-10 μM), Azacytidine (0.15-10 μM), Decitabine (0.15-10 μM), or Cytarabine (0.1-5 μM) for 48-72 h. Following the treatment, Cell Proliferation Reagent WST-1 solution (#05015944001; Sigma-Aldrich, St. Louis, MO) was added (1:10 final dilution) and incubated for 2-3 h. Absorbance was measured at 440 nm and 650 nm (reference wavelength) by SpectraMax M5 Multimode Plate Reader (RRID:SCR_020300; Molecular Devices, San Jose, CA). Following background subtraction, the absorbance values were presented as % viability relative to the vehicle (DMSO) control.

Drug synergy analysis

Dose-response matrices generated from percent cell viability data after drug combination treatment were used to compute synergy scores. Inhibition effect in terms of fraction affected (Fa) was scored from 0 to 1, where a score of '0' represented no effect and a score of '1' represented 100% effect. CompuSyn software (version 1.0; T. C. Chou and N. Martin, Memorial Sloan-Kettering Cancer Centre, New York) was used to calculate the combination index (CI) and quantitatively establish the effect of drug interactions.[2] CI value of <1 indicates synergism between the drug combinations.

Muse apoptosis assay

Apoptosis in primary AML cells and AML cell lines after the treatment was measured in terms of Annexin V levels by Muse Annexin V & Dead Cell Kit (Cytek, Cat# MCH100105) as per the manufacturer's instructions. For each sample, at least 2000 events were acquired using CyTekBio: Guava Muse Cell Analyzer (RRID:SCR_020252) and represented as apoptosis (Annexin V positive cells) relative to vehicle 'Control'.

Lentiviral shRNA transduction

Lentiviral particles containing four unique shRNAs against human *CSNK2A1* (#TL320317V) and *CSNK2A2* (#TL320318V) were obtained from OriGene Technologies (Rockville, MD). Molm13-VR AML cells were transduced in a 12-well plate with shRNA lentiviral particles for either *CSNK2A1* or *CSNK2A2* at 1-3 Multiplicity of Infection (MOI) using 8 µg/mL of polybrene (#TR-1003-G; Millipore Sigma, Rockville, MD) and spinoculation at 1600 rpm for 60 min at 32 ^{o}C. The cells were sorted for GFP by flow cytometry under BSL-2 conditions using a BD FACSAria SORP (BD Biosciences, San Jose, CA) instrument in Penn State College of Medicine's Flow Cytometry Core (RRID:SCR_021134) 72 h post-transduction and screened for target gene knockdown by qPCR and western blotting as described below. The shRNAs with highest knockdown efficiency were selected to achieve the double knockdown of both *CSNK2A1* and *CSNK2A2* genes in the target AML cell lines. Cells transduced with scramble shRNA were used as controls for subsequent experiments, including western blotting and apoptosis assays.

RNA sequencing analysis

Total RNA was isolated from AML cell lines (Molm13 and Molm13-VR) and PDX (2016-7) cells after 24 h of treatment with DMSO (vehicle), CX-4945, VEN, and CX+VEN combination using TRIzol reagent (#15596018; Invitrogen, Carlsbad, CA). RNA quality and integrity were assessed using an Agilent 2100 Bioanalyzer (Agilent Technologies, Palo Alto, CA). Paired-end RNA sequencing was performed on the NovaSeq X Plus platform (Novogene, Sacramento, CA). The reads were processed, aligned to the human reference genome (hg38), and visualized as previously described.[3] Briefly, differential expression analysis was conducted using edgeR (RRID:SCR_012802), where a quasi-likelihood negative binomial generalized log-linear model was fitted to the data using the glmQLFTest function. Prior to modeling, the raw count data were normalized using the trimmed mean of M-values (TMMs) method. The Benjamini–Hochberg (BH) procedure was applied for multiple testing

correction, and genes with an adjusted p-value below 0.05 and fold change above 1.5 were considered as significantly differentially expressed. The principal component analysis (PCA) plots were generated using SRplot web server (RRID:SCR_025904).[4] Hierarchical gene clustering (k-means) analysis with normalized count data and functional enrichment analysis (MSigDB hallmark gene, GO-biological process) was performed using a web-based RNAseqChef platform.[5] Enrichment of gene signatures for diseases/drugs in differentially expressed genes was analyzed using Enrichr web server (RRID:SCR_001575).[6]

Quantitative PCR

Total RNA was extracted from AML cell lines (Molm13 and Molm13-VR) using TRIzol reagent and reverse-transcribed into cDNA using the iScript cDNA Synthesis Kit (#1708891; Bio-Rad Laboratories, Hercules, CA). cDNA amplification was performed using the PowerTrack SYBR Green Master Mix (#A46110; Thermo Fisher Scientific, Waltham, MA). The thermal cycling program consisted of 40 cycles of denaturation at 94 °C for 30 sec and annealing/extension for 30 sec at 60 °C. All qPCR reactions were performed in triplicate within the same run. *GAPDH* was used as an internal control for normalization and relative expression levels were determined by the $2^{-\Delta\Delta Ct}$ method. Primer sequences used in this study are listed in **Table S4**.

BH3 profiling and dynamic BH3 profiling (DBP)

BH3 profiling involves determining the sensitivity of AML cells to BH3 peptides without drug perturbation, whereas dynamic BH3 profiling (DBP) determines the sensitivity after exposure to CX-4945. Intracellular BH3 profiling was performed as described earlier.[7] Exponentially growing AML cell lines (Molm13, Molm13-VR) were first stained with viability dye (1:1000), Zombie Aqua Fixable Viability Kit (#423102; BioLegend), washed with phosphate-buffered saline (PBS), and then resuspended in 50 µL of MEB buffer (150 mM mannitol, 150 mM KCl, 10 mM HEPES-KOH, 5 mM succinate, 20 µM EDTA, 20 µM EGTA, 0.1% protease free BSA, final pH 7.5). BH3 peptides including BIM, BID, and PUMA (BIOSYNTH, Gardner, MA) were prepared 2X the desired concentration in MEB buffer supplemented with 0.002 % digitonin. The cells were mixed with 50 µL BH3 peptides (0.1 – 100 µM) or 50 µM alamethicin (ALA), incubated for 90 min at room temperature and then fixed. Following neutralization, anti–cytochrome c antibody (#612310; BioLegend, RRID:AB_2565241) was added at a 1:2000 final dilution in staining buffer and incubated at 4°C overnight before acquisition with a BD LSRFortessa flow cytometer (BD Biosciences, San Jose, CA). ALA was used as a positive control for cytochrome c (Cyt c) release.

For DBP, exponentially growing AML cell lines (Molm13 and Molm13-VR) were treated with 10 μM CX-4945 or the equivalent DMSO (vehicle) for 16 h. After treatment, the cells were collected for subsequent BH3 profiling as described above and mixed with BH3 peptides (final concentration of 1 μM for BIM, PUMA and 10 μM of BID). Sensitivity to BH3 peptides was measured as percent cytochrome c release loss as determined by FACS and calculated using the following equation: [cytochrome c loss = 100 − (% of cells within the cytochrome c retention gate)]. The readout of BH3 profiling and DBP is a change in mitochondrial priming defined as "% delta priming" (% delta priming = % cytochrome c loss [drug/peptide] − % cytochrome c loss [DMSO]). DMSO was used as a negative control for cytochrome c release, whereas ALA treatment was used as a positive control for 100% cytochrome c release.

Flow cytometry

To assess apoptosis in AML cells, we used the PE Annexin V Apoptosis Detection Kit with 7-AAD (#640934; BioLegend, San Diego, CA) per manufacturer's protocol. Briefly, human AML cell lines and PDX cells were treated with vehicle (DMSO), CX-4945, VEN, or CX+VEN at the indicated doses. After 24 h of treatment, the cells were washed twice with ice-cold PBS and resuspended in 1X Annexin V binding buffer before adding 5 μL of each PE-Annexin V and 7-AAD. The cells were incubated for 20 min at room temperature in the dark and then analyzed using a BD FACSCalibur flow cytometer (BD Biosciences, San Jose, CA). The data are represented as a fold change in the percentage of apoptotic (Annexin V +Ve) cells relative to the vehicle (DMSO) control.

For immunophenotyping, AML cells (cell lines, primary cells, and spleen or bone marrow cells harvested from xenograft mice) were collected (0.2-1 $x10^6$) by centrifugation and washed with ice-cold PBS before addition of viability dye (1:1000) from Zombie Aqua Fixable Viability Kit (#423102; BioLegend). After 20 min incubation in the dark at room temperature, cells were washed with FACS staining buffer (Dulbecco's PBS with 3% FBS) prior to blocking the mouse or human Fc receptor (BD Biosciences, San Jose, CA) for 10 min. The cells were then stained with an antibody cocktail for 30 min in the dark at 4 ^oC and washed twice with FACS staining buffer before data acquisition using a BD LSRFortessa flow cytometer (BD Biosciences, San Jose, CA). To analyze apoptosis in AML subpopulations, the cells stained with the antibody cocktail were incubated with BV711-Annexin V (#563972; BD Biosciences) and 7AAD (#420404, BioLegend) for 20 min at room temperature in the

dark before data acquisition using a flow cytometer. Data analysis was performed using the FlowJo v10.10 Software (BD Life Sciences, RRID:SCR_008520).

The frequencies of different cell types in the bone marrow and spleen samples were calculated using FACS analysis as described previously.[3] Absolute cell numbers were calculated based on the total cell numbers obtained from the trypan blue exclusion assay using a CellDrop automated cell counter (DeNovix, Wilmington, DE). The absolute number of cells in the populations of interest was calculated using the formula: absolute cell number = (number of cells in gate/number of cells in live cells) × total cell number in organs (BM or spleen). All antibody information, including clones and vendors, is summarized in **Table S5**.

Immunoblotting

AML cell lines were seeded at a density of 4 x 10^5 cells/mL in a 6-well plate and left untreated or treated with vehicle (DMSO), CX-4945, VEN, or CX+VEN at the indicated doses for 24 h. The cells were collected by centrifugation, washed with ice-cold PBS, and then whole-cell lysates were prepared using 1X cell lysis buffer (#9803; Cell Signaling Technology, Danvers, MA) supplemented with 1 mM PMSF protease inhibitor (#36978; Thermo Scientific) and phosphatase inhibitor cocktail (#P5726; Sigma-Aldrich). After quantification of protein concentration using a BCA assay kit (#23225; Thermo Fisher Scientific), an equal amount of protein (10-20 µg) from each sample was denatured at 95 ºC for 5 min in reducing SDS loading buffer (#7722; Cell Signaling Technology), subjected to gel electrophoresis using 4–20% Mini-PROTEAN TGX precast protein gels (RRID:SCR_008426, Bio-Rad Laboratories, Hercules, CA) and transferred to Immobilon-FL PVDF membrane (#IPFL00010; Millipore Sigma). Following blocking with 5% non-fat dry milk in Tris-buffered saline with 0.1% Tween-20 (TBST), the membranes were incubated with primary antibodies (listed in **Table S6**) overnight at 4 ºC. After three TBST washes for each 5 min, the blots were incubated with secondary antibodies either anti-rabbit (#7074, Cell Signaling, RRID:AB_2099233) or anti-mouse IgG–horseradish peroxidase (HRP) conjugates (#7076, Cell Signaling, RRID:AB_330924) for 45-60 min at room temperature and washed three times in TBST. SuperSignal West Femto Maximum Sensitivity Substrate (#34095, Thermo Scientific) was used as enhanced chemiluminescent (ECL) substrate and the signals were detected using Azure 500 imaging station (Azure Biosystems, Dublin, CA) or Bio-Rad ChemiDoc MP imaging system (RRID:SCR_008426, Bio-Rad Laboratories, Hercules, CA). Representative blots from at least two or three independent experiments are presented.

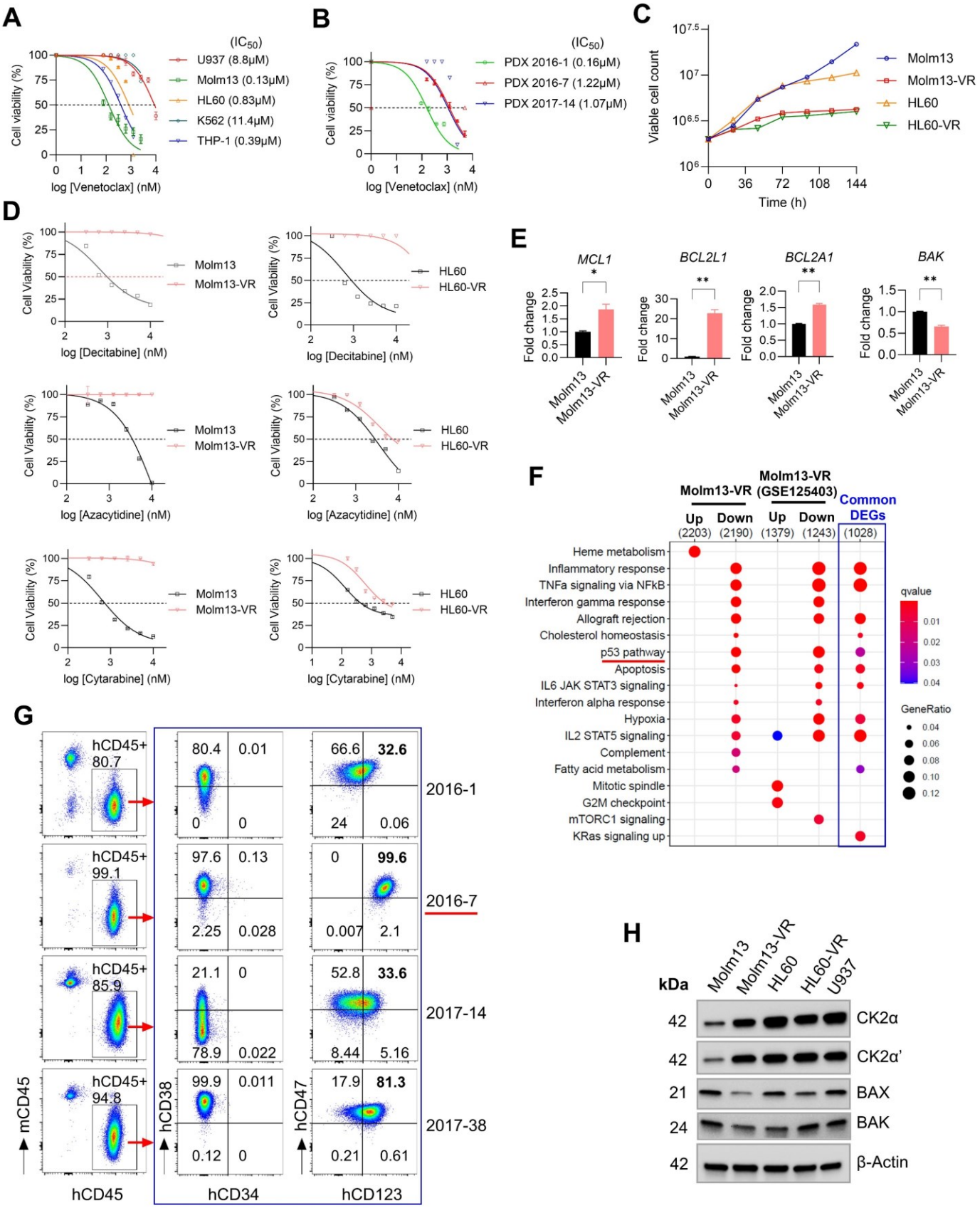
In vivo efficacy experiments

All mouse care and experiments were conducted in accordance with the protocols approved by the Institutional Animal Care and Use Committee (IACUC). To test the *in vivo* efficacy of CX-4945 and VEN combination, we used both cell line-derived xenograft (CDX) and patient-derived xenograft (PDX) mouse models. To establish CDX and PDX models, Molm13-VR ($0.25x10^6$ cells/mouse) and U937 ($1x10^4$ cells/mouse) AML cell lines and PDX 2016-7 ($0.5x10^6$ cells/mouse) cells were injected via tail vein into 6-8-week-old NOD Cg-Rag1tm1Mom Il2rgtm1Wjl Tg(CMV-IL3,CSF2,KITLG)1Eav/J (NRG-S) mice (The Jackson Laboratory, Bar Harbor, ME; RRID:IMSR_JAX:024099). Mice (both sexes) were randomized into four experimental groups: vehicle (control), CX-4945 (100 mg/kg, p.o., twice daily), VEN (12.5 mg/kg, p.o., once daily), and the CX+VEN combination. The CX-4945 solution was freshly prepared in sodium phosphate buffer (pH=7.8) and passed through a 0.22 μm filter before every dosing. The VEN solution was prepared as per the manufacturer's instructions by sequential addition of 5% DMSO, 40% PEG300, 5% Tween-80, and 50% saline. We included an extra cohort of PDX mice from all the experimental groups to harvest blood and tissue (spleen and bone marrow) after two weeks of treatment for analysis by flow cytometry and immunoblotting. Drug treatment was initiated one week after cell transplantation and continued until study termination. The mice were regularly monitored, and a complete blood count (CBC) of peripheral blood was performed every week until the end of the experiment using a Hemavet 950FS analyzer (Drew Scientfic, Plantation, FL). After the treatment period, the main study cohort mice were monitored for overall survival and subjected to Kaplan–Meier analysis.

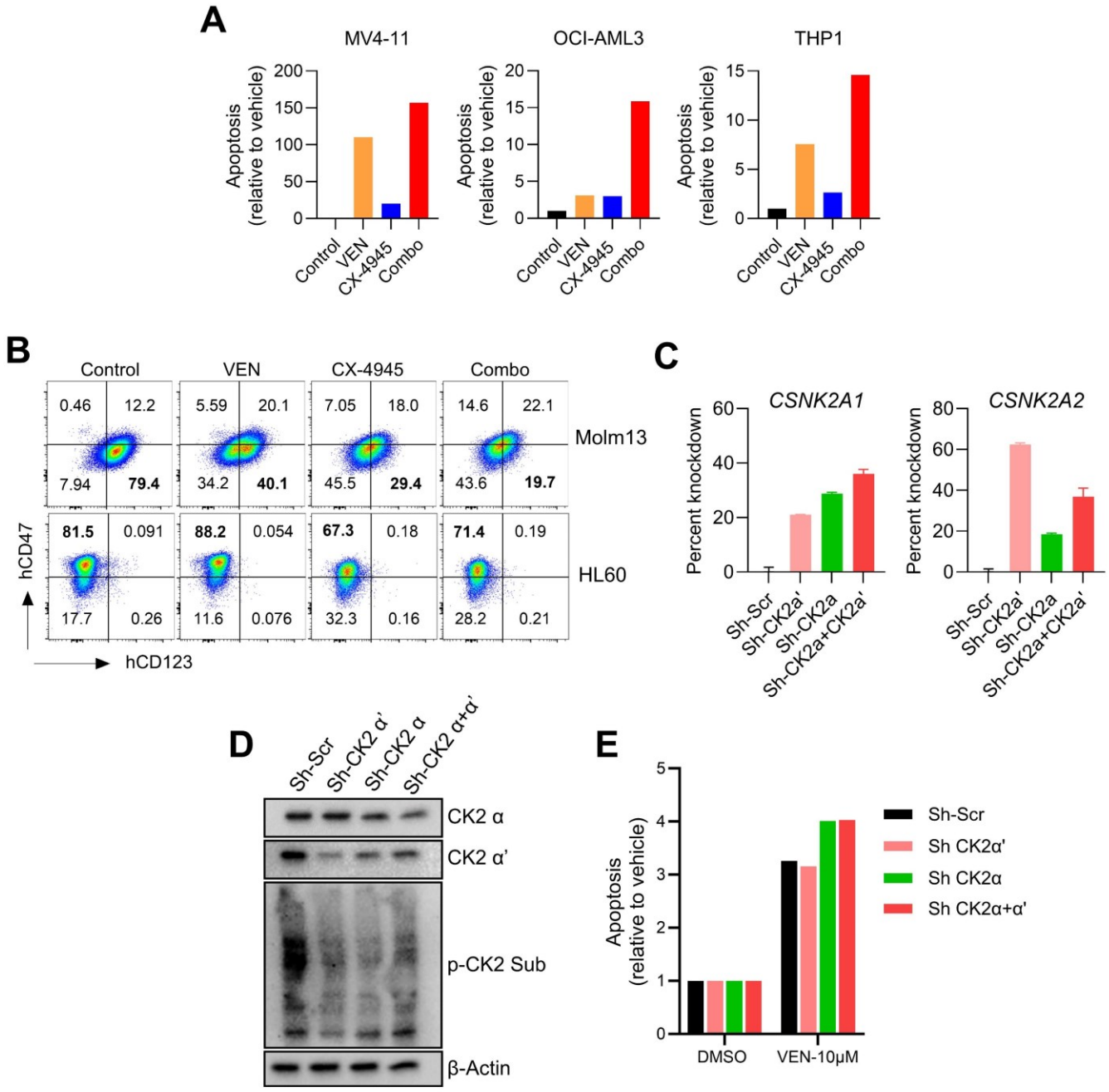
Statistical analysis

Statistical tests were performed using GraphPad Prism 10 software (RRID:SCR_002798). Comparisons between two groups were performed using unpaired Student's t-test, whereas comparisons among three or more groups were evaluated by analysis of variance (ANOVA) test. The Gehan-Breslow-Wilcoxon test was used to compute p-value for Kaplan-Meier survival analysis. All data are represented as the mean ± standard error of the mean (SEM) or standard deviation (SD) from two or three independent experiments, and a p-value less than 0.05 considered as statistically significant. Details of the post hoc tests if any used to calculate p-values are provided in the respective figure legends.

Supplementary Figures

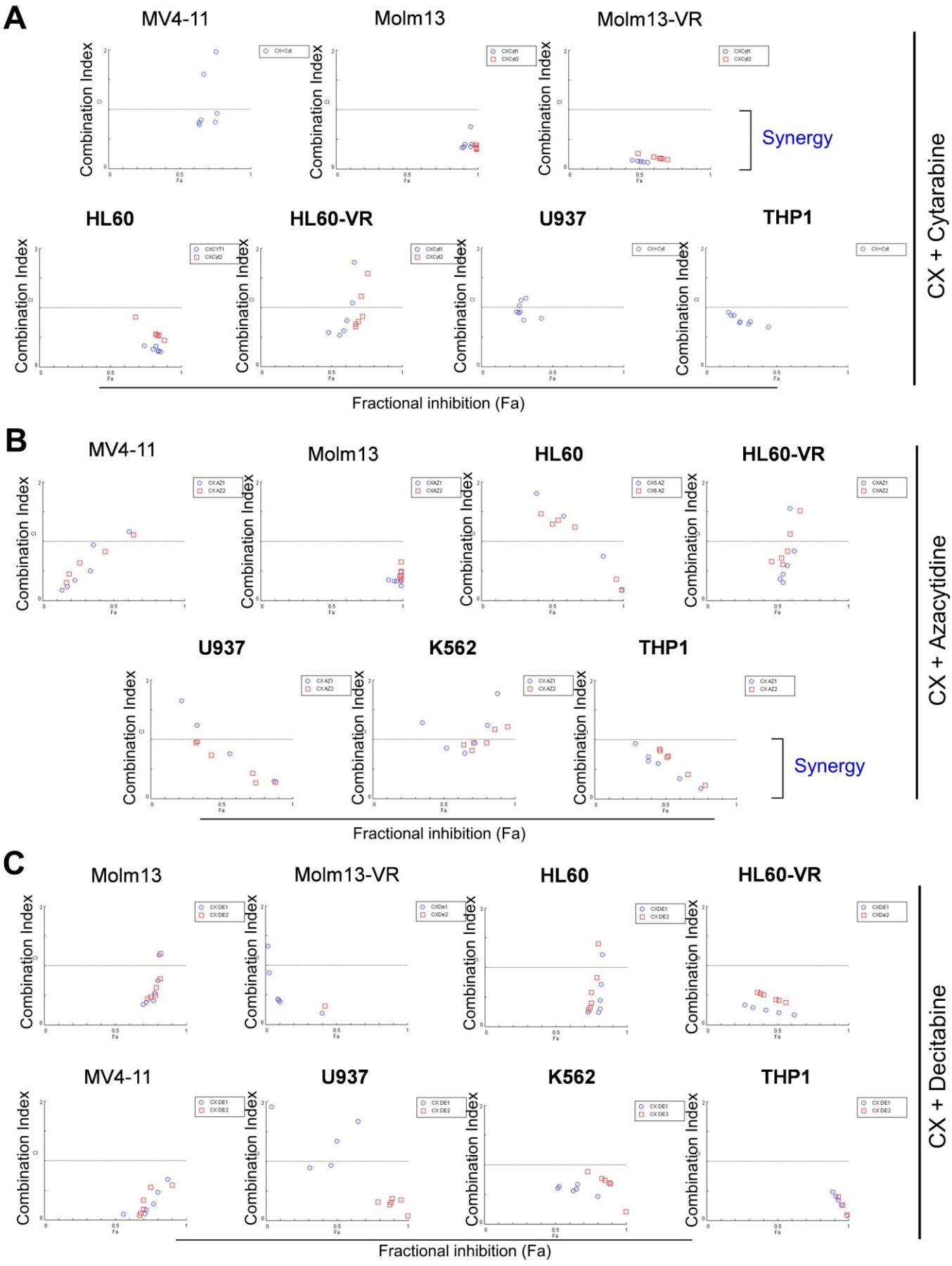


Supplementary Figure 1: The characterization of venetoclax-resistant AML cell lines and cytotoxic effect of different standard drugs on AML cell lines and PDX cells. A-B) AML cell lines (A) and PDX cells (B) were treated with different concentrations of venetoclax for 48 h and accessed for cell viability using WST assay. The IC_{50} doses of venetoclax was indicated next to the corresponding legend for AML cell lines. **C)** The proliferation of venetoclax susceptible (parental) and VEN-resistant (VR) AML cells was analyzed for 6 days using CellDrop automated cell counter. **D)** The cross resistance of venetoclax-resistant AML cells to AML standard cytotoxic therapy agents (Decitabine, 5-Azacytidine, Cytarabine) was tested against different concentrations for 48h and assessed for cell viability by WST assay. **E)** The basal level expression of indicated genes was assessed in parental and VEN-resistant Molm13 AML cell lines by qRT-PCR. The data are presented as mean ± SEM (n=3 tech replicates from a representative run). *p<0.05, **p<0.01 and ****p<0.0001 by unpaired t-test (Welch's correction). **F)** Differential gene expression analysis by RNA-seq in Molm13-VR (MVR) compared to parental Molm13 (M) cell line was performed. Dot plot showing the top-ranked functional pathways (MSigDB hallmark gene set) enriched in differentially regulated genes (fold-change >1.5 and adj-p <0.05) in Molm13-VR cells when compared to parental cells. The molecular gene signatures of our Molm13-VR cells are similar and comparable to previously reported study (GSE125403). **G)** The basal level surface expression of markers for LSCs (CD34, CD38) and chemoresistance (CD47, CD123) were analyzed using flow cytometry in different AML PDX cells. **H)** The basal level expression of indicated target proteins in different AML cell lines was assessed by immunoblotting.

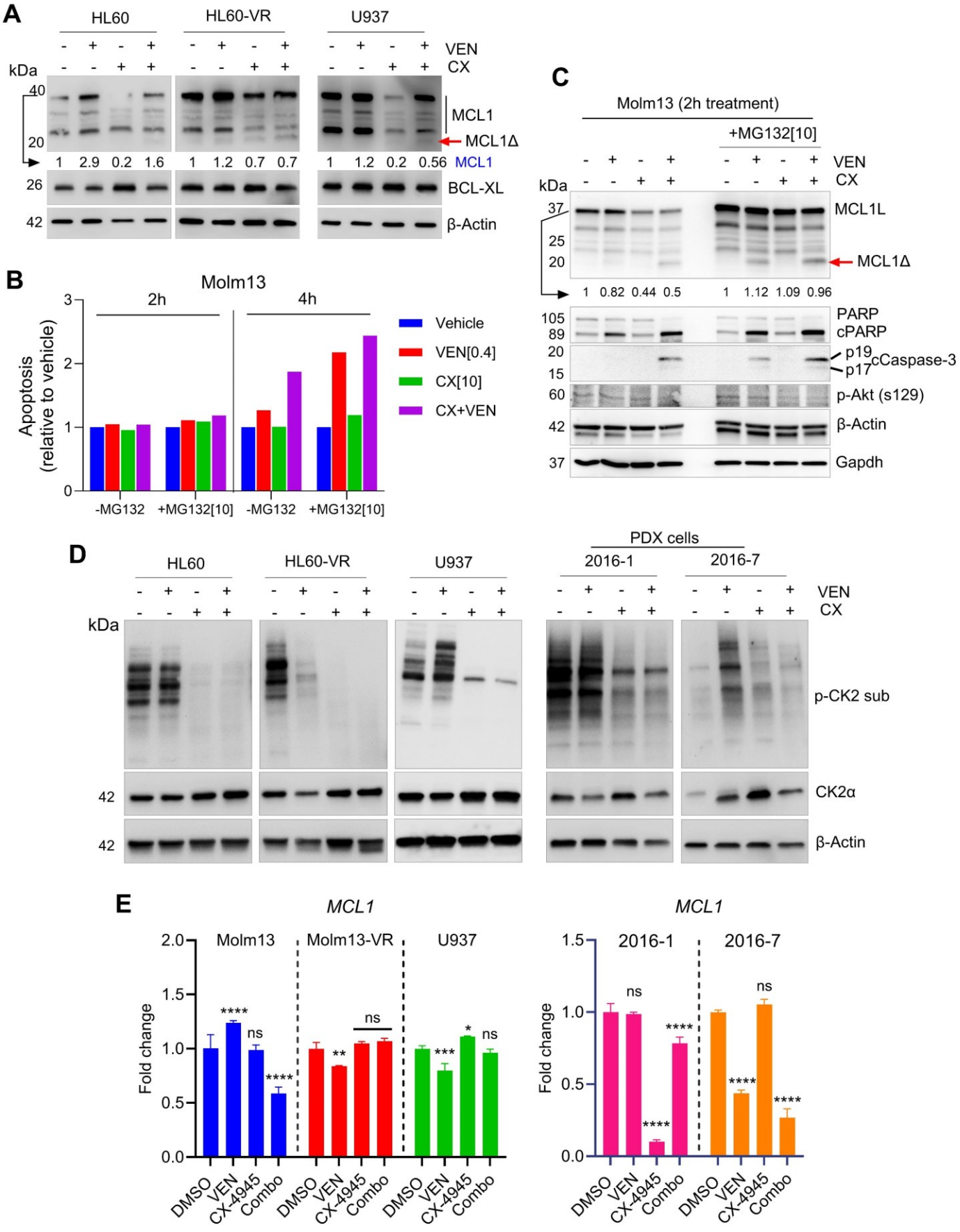


Supplementary Figure 2: CK2 inhibition augments cytotoxic effect of VEN in AML cell lines. A) AML cell lines (MV4-11, OCI-AML3, THP1) were treated with CX-4945 and VEN alone or in combination for 24 h and stained with Annexin V/7AAD for analyzing apoptosis by flow cytometry. THP1 is a TP53 mutated AML cell line. Relative apoptosis was calculated by normalizing to vehicle treated cells. **B)** AML cell lines (HL-60, HL-60/VR, U937) were treated with CX-4945 and VEN alone or in combination for 24 h and the surface expression of chemoresistance markers (CD47 and CD123) was analyzed by flow cytometry. A representative density plot shows hCD123 and hCD47 levels in parental (Molm13 and HL60) AML cells after the drug treatment. **C and D)** Molm13-VR cells were transduced with lentiviral particles expressing GFP-tagged shRNAs specific to *CSNK2A1*

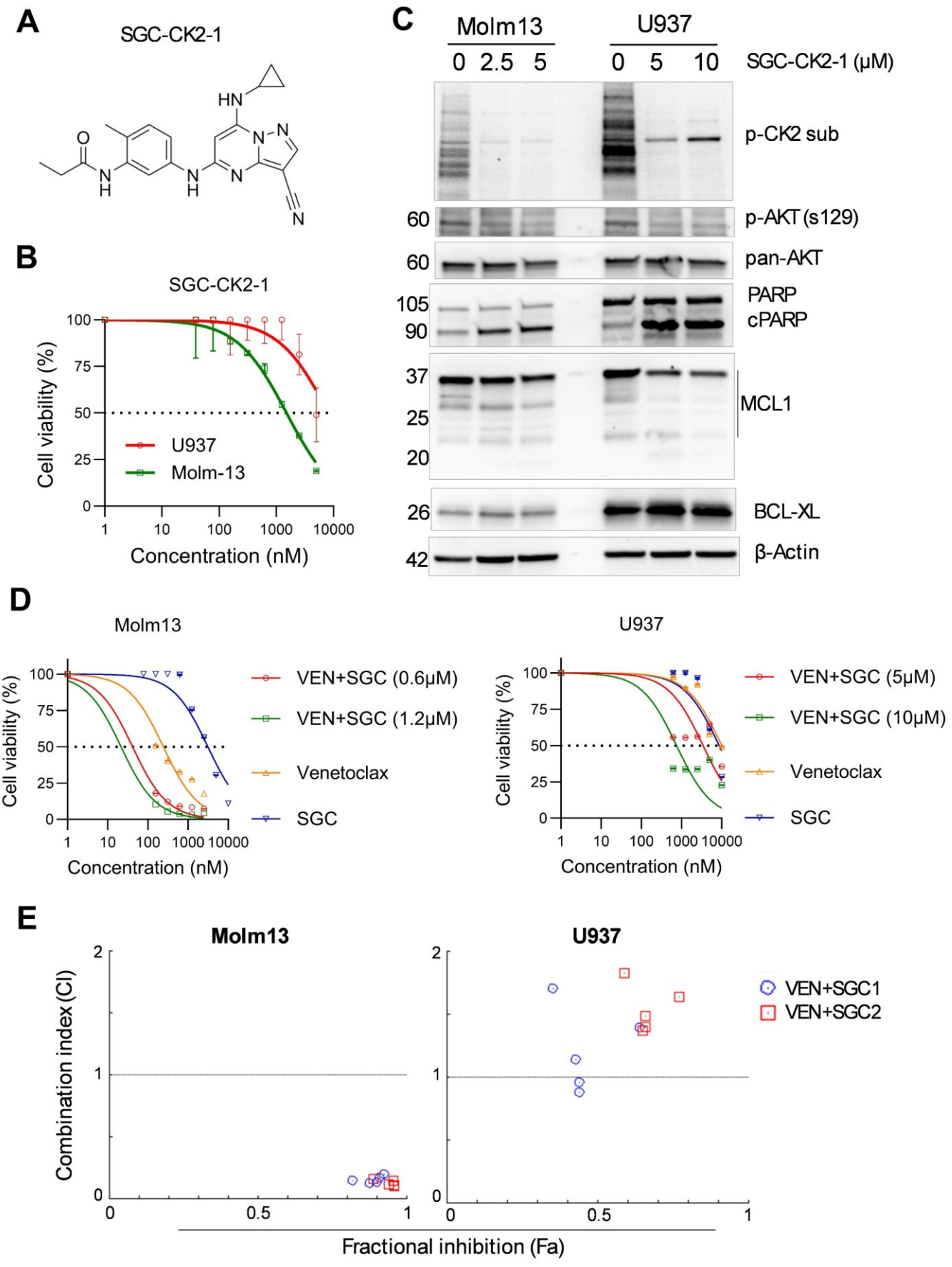
and *CSNK2A2* alone or together in the presence of polybrene (8 µg/mL). The cells positive for GFP were sorted and tested for target gene knockdown using qPCR (**C**) and western blotting (**D**). β-Actin was used as a loading control for western blotting experiments. **E)** The relative apoptosis in Molm13-VR cells after knockdown of *CSNK2A1* and *CSNK2A2* genes alone or combination was analyzed after 24 h treatment with either vehicle (DMSO) or VEN (10µM) using muse cell analyzer.


A
MV4-11
Molm13
Molm13-VR
Combination Index
Synergy
HL60
HL60-VR
U937
THP1
CX + Cytarabine
Fractional inhibition (Fa)
B
MV4-11
Molm13
HL60
HL60-VR
U937
K562
THP1
Combination Index
Synergy
CX + Azacytidine
Fractional inhibition (Fa)
C
Molm13
Molm13-VR
HL60
HL60-VR
MV4-11
U937
K562
THP1
Combination Index
CX + Decitabine
Fractional inhibition (Fa)

Supplementary Figure 3: CX-4945 synergizes with AML standard cytotoxic therapy agents in AML cell lines. A-C) AML cell lines were treated with CX-4945 in combination with AML standard cytotoxic therapy agents (Cytarabine, 5-Azacytidine) for 48 h, or Decitabine for 72 h. Cell viability was assessed using WST reagent and cell viability was calculated relative to vehicle-treated cells as 100%. Combination index (CI) plots presenting fractional inhibition (Fa) and CI values in different AML cell lines after CX-4945 combination with Cytarabine (**A**), 5-Azacytidine (**B**), and Decitabine (**C**). CI values of <1 (below the line) indicate synergism between the drug combinations. Cell lines carrying mutations in *TP53* were indicated in bold.


A
HL60
HL60-VR
U937
VEN
CX
kDa
40
20
MCL1
MCL1Δ
1 2.9 0.2 1.6 1 1.2 0.7 0.7 1 1.2 0.2 0.56 MCL1
26
BCL-XL
42
β-Actin
B
Molm13
2h
4h
Apoptosis (relative to vehicle)
Vehicle
VEN[0.4]
CX[10]
CX+VEN
-MG132
+MG132[10]
-MG132
+MG132[10]
C
Molm13 (2h treatment)
+MG132[10]
VEN
CX
kDa
37
25
20
MCL1L
MCL1Δ
1 0.82 0.44 0.5 1 1.12 1.09 0.96
105
89
PARP
cPARP
20
15
p19
p17
cCaspase-3
60
p-Akt (s129)
42
β-Actin
37
Gapdh
D
HL60
HL60-VR
U937
PDX cells
2016-1
2016-7
VEN
CX
kDa
p-CK2 sub
42
CK2α
42
β-Actin
E
MCL1
Molm13
Molm13-VR
U937
Fold change
DMSO
VEN
CX-4945
Combo
MCL1
2016-1
2016-7
Fold change
DMSO
VEN
CX-4945
Combo

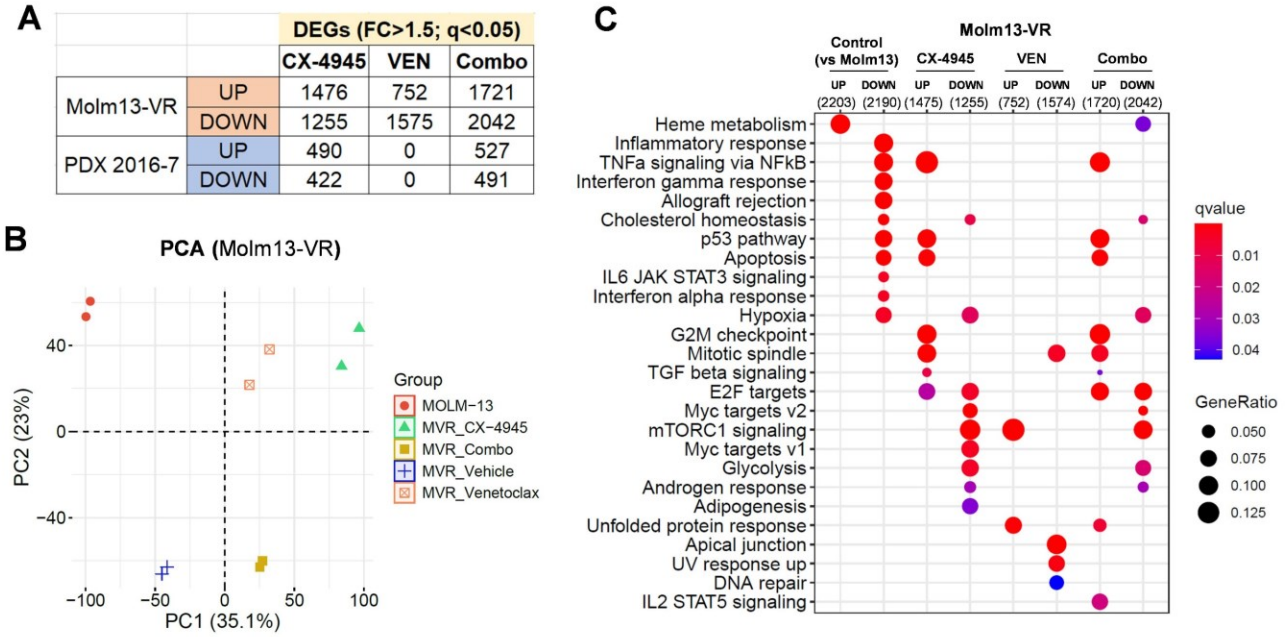
Supplementary Figure 4: Effect of CX-4945 and VEN combination on MCL1 and BCL-XL in AML cells. A) The levels of MCL1 and BCL-XL were measured by immunoblotting in AML cell lines after 24h of treatment with IC_{50} doses of CX-4945 and VEN alone or in combination. The levels of MCL1L were quantified relative to β-Actin and normalized to vehicle control cells. The shortest band indicated by red arrow denotes proteolytic fragment of MCL1L protein (MCL1Δ). **B)** Analysis of relative apoptosis (Annexin V) in Molm13 AML cells following 4h treatment with CX, VEN alone or in combination with or without proteasomal inhibitor MG132 (10 μM). Representative data from two independent experiments are presented. **C)** Immunoblotting analysis of Molm13 AML cell lines after 2 h of treatment with CX-4945 and VEN alone or in combination with or without proteasomal inhibitor MG132 (10 μM). The levels of MCL1L were quantified relative to Gapdh and normalized to vehicle control cells. The shortest band indicated by red arrow denotes proteolytic fragment of MCL1L protein (MCL1Δ). 'cPARP' and 'cCaspase-3' denote cleaved PARP and cleaved Caspase-3, respectively. **D)** Immunoblotting analysis of AML cell lines after 24h of treatment with CX-4945 and VEN alone or in combination. β-Actin was used as a loading control. Blots from representative experiments are shown in '**A**, **C** & **D**'. **E)** Quantification of *MCL1* transcript levels after treatment with CX-4945 and VEN alone or in combination for 24h in indicated AML cell lines and PDX cells by qPCR. The data are presented as mean ± SD (n=3 replicates from a representative run). *p<0.05, **p<0.01, ***p<0.001, and ****p<0.0001 by two-way ANOVA (Tukey's multiple comparisons test).

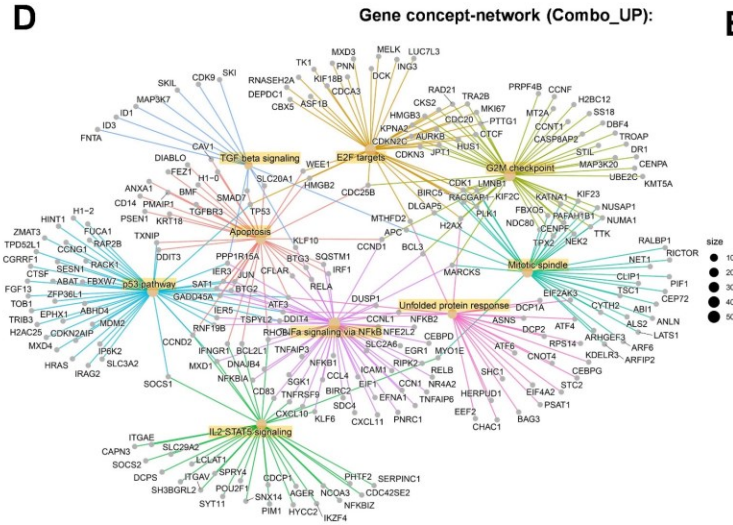

A
SGC-CK2-1
B
SGC-CK2-1
Cell viability (%)
Concentration (nM)
U937
Molm-13
C
Molm13
U937
0 2.5 5
0 5 10
SGC-CK2-1 (μM)
p-CK2 sub
p-AKT (s129)
pan-AKT
PARP
cPARP
MCL1
BCL-XL
β-Actin
D
Molm13
U937
VEN+SGC (0.6μM)
VEN+SGC (1.2μM)
Venetoclax
SGC
VEN+SGC (5μM)
VEN+SGC (10μM)
E
Molm13
U937
Combination index (CI)
Fractional inhibition (Fa)
VEN+SGC1
VEN+SGC2

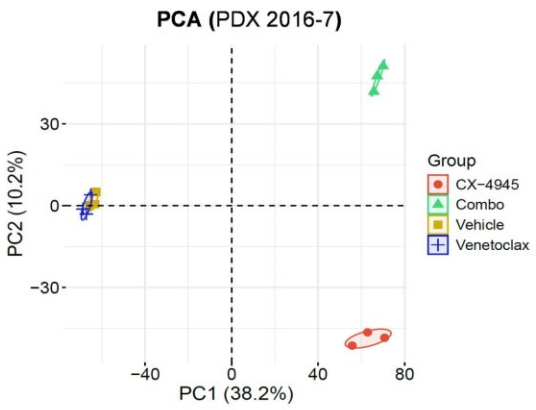
Supplementary Figure 5: CK2 selective inhibitor SGC-CK2-1 downregulate MCL1 and synergize with VEN in AML cells. A) Structure of SGC-CK2-1, a potent and highly specific CK2 inhibitor. **B)** Dose response curves for SGC-CK2-1 in Molm13 (inherently VEN-sensitive) and U937 (inherently VEN-resistant) AML cell lines after treatment with different concentrations for 48 h and assessed for cell viability using WST assay. **C)** Immunoblotting analysis of indicated AML cell lines after 24 h of treatment with SGC-CK2-1. β-Actin was used as a loading control. Blots from representative experiments are shown. **D)** AML cell lines (Molm13, U937) were treated with SGC-CK2-1 and VEN alone or in combination with indicated doses for 48 h. Cell viability was assessed using WST reagent and cell viability was calculated relative to vehicle-treated cells as 100%. **E)** Combination index (CI) plots presenting fractional inhibition (Fa) and CI values in indicated AML cell lines after 48 h treatment with VEN (0.1-10 μM) in combination with two doses of SGC-CK2-1 (shown in '**D**'). CI values of <1 (below the line) indicate synergism between SGC-CK2-1 and VEN combination.

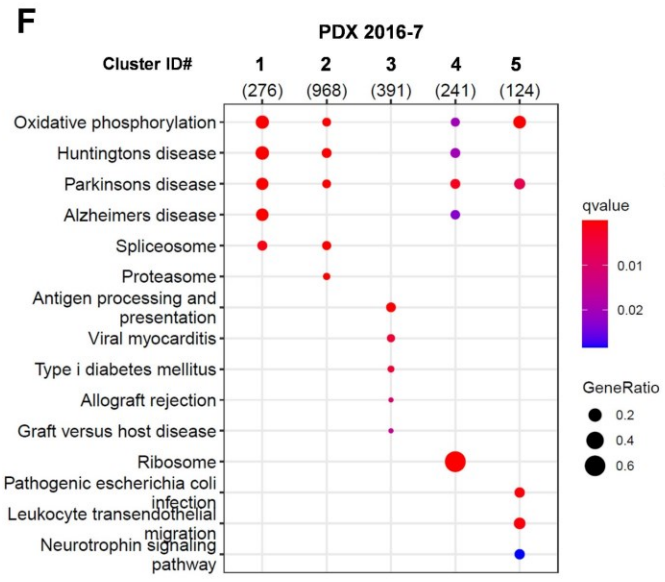
A

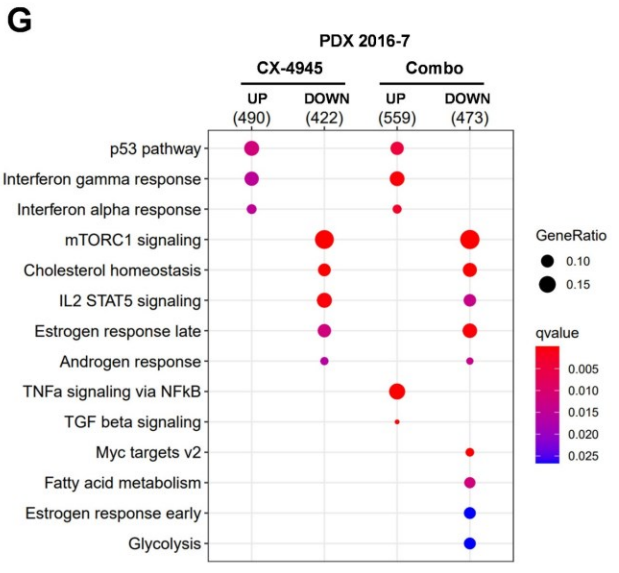
		DEGs (FC>1.5; q<0.05)		
		CX-4945	VEN	Combo
Molm13-VR	UP	1476	752	1721
	DOWN	1255	1575	2042
PDX 2016-7	UP	490	0	527
	DOWN	422	0	491



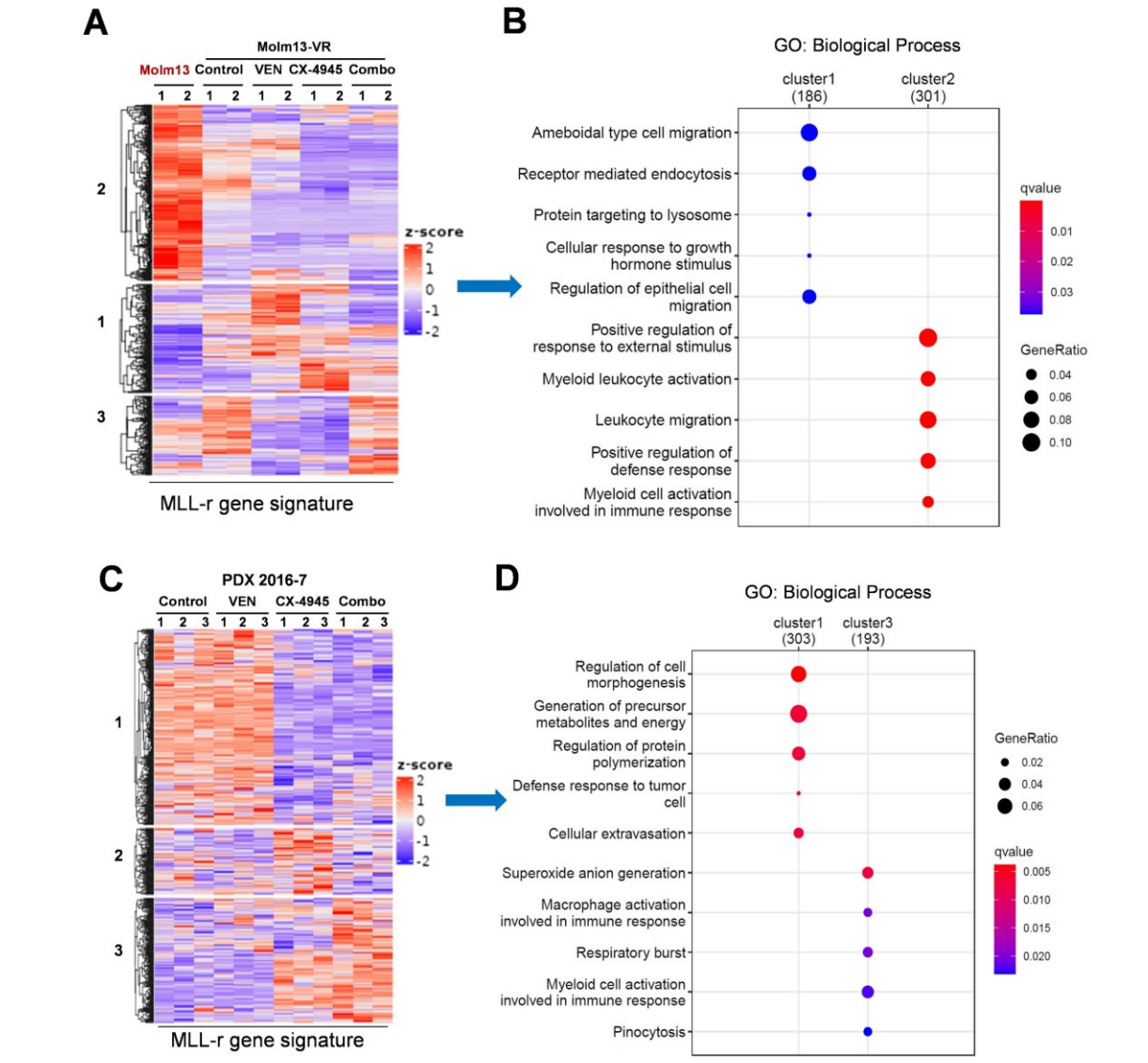




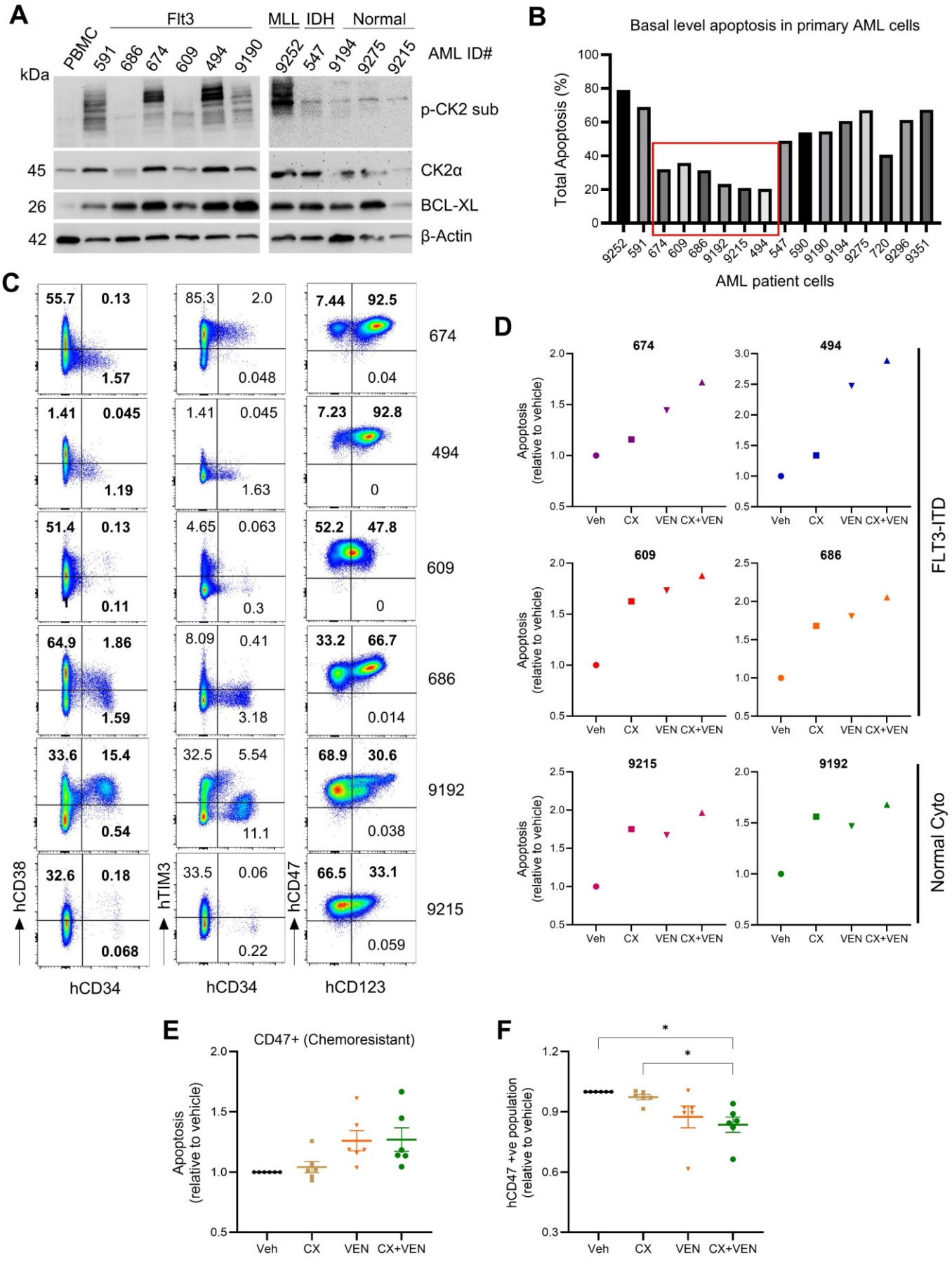




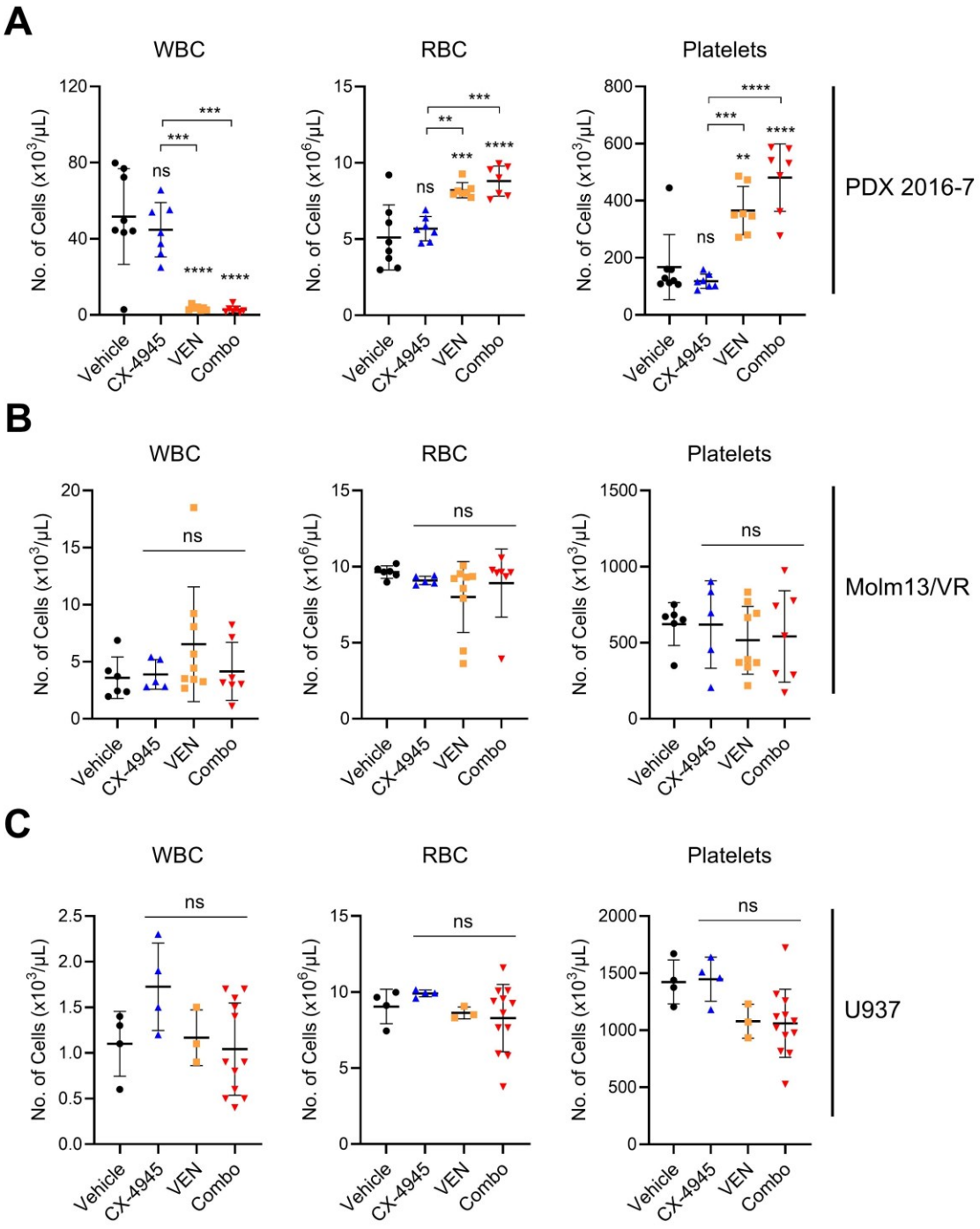
Supplementary Figure 6: Differential gene expression and overrepresentation analysis with AML cells transcriptome after CX and VEN combination treatment. A) Summary plot showing the number of differentially expressed genes (DEGs) in Molm13-VR and PDX 2016-7 cells after 24 h of treatment with CX-4945 (CX), venetoclax (VEN), and CX+VEN combination (Combo). **B)** Principal component analysis (PCA) plot showing the distribution of Molm13 (parental) versus Molm13-VR (with and without drug treatment for 24h) AML cell lines (n=2 out of three replicates). **C)** Dot plot displaying the top-ranked functional pathways (MSigDB hallmark gene set) overrepresented in differentially expressed genes (fold change >1.5 and adj-p <0.05) in Molm13-VR (vs. Molm13) and Molm13-VR cells after 24 h of drug treatment. **D)** Gene-Concept network analysis depicting the gene-to-gene interconnection in the top-ranked functional pathways (MSigDB hallmark gene set) overrepresented with significantly differentially expressed genes in Molm13-VR cells with CX+VEN combination treatment (control vs. Combination). Node size refers to the number of genes in the enriched pathway. Genes shared between edges refer to terms belonging to multiple pathophysiological categories. **E)** Principal component analysis (PCA) plot showing the distribution of PDX 2016-7 (with and without drug treatment for 24h) AML cells (n=3). **G)** Heatmap showing the hierarchical clustering (k-means) of most variable genes (n=2000) in PDX 2016-7 AML cells transcriptome. **F and G)** Dot plot displaying the top-ranked biological processes (gene ontology) overrepresented in different gene clusters obtained with the hierarchical clustering (k-means) of most variable genes (n=2000) as shown in '**Figure 6C**' (**F**) or the differentially expressed genes (fold change >1.5 and adj-p <0.05) in PDX 2016-7 AML cells after 24 h of drug treatment (**G**).


A
Molm13-VR
Molm13 Control VEN CX-4945 Combo
1 2 1 2 1 2 1 2 1 2
2
1
3
z-score
2
1
0
-1
-2
MLL-r gene signature
B
GO: Biological Process
cluster1 (186)
cluster2 (301)
Ameboidal type cell migration
Receptor mediated endocytosis
Protein targeting to lysosome
Cellular response to growth hormone stimulus
Regulation of epithelial cell migration
Positive regulation of response to external stimulus
Myeloid leukocyte activation
Leukocyte migration
Positive regulation of defense response
Myeloid cell activation involved in immune response
qvalue
0.01
0.02
0.03
GeneRatio
0.04
0.06
0.08
0.10
C
PDX 2016-7
Control VEN CX-4945 Combo
1 2 3 1 2 3 1 2 3 1 2 3
1
2
3
z-score
2
1
0
-1
-2
MLL-r gene signature
D
GO: Biological Process
cluster1 (303)
cluster3 (193)
Regulation of cell morphogenesis
Generation of precursor metabolites and energy
Regulation of protein polymerization
Defense response to tumor cell
Cellular extravasation
Superoxide anion generation
Macrophage activation involved in immune response
Respiratory burst
Myeloid cell activation involved in immune response
Pinocytosis
GeneRatio
0.02
0.04
0.06
qvalue
0.005
0.010
0.015
0.020
E
NIBR DRUGseq 2025 up
Molm13-VR (Combo_UP)
CID24748573 SILMITASERTIB IC-18-TY61 BAID24 10UM
CX-4945 (CK2 inhibitor)
CID131953885 EIF4A3-IN-2 HD-89-HC56 BAID12 10UM
eIF4A3 (RNA helicase) inhibitor
CID49784945 IZORLISIB BF-26-MB27 BAID40 10UM
PI3K inhibitor
CID5329102 SUNITINIB BB-09-GD09 BAID28 10UM
Multi-tyrosine kinase inhibitor
F
NIBR DRUGseq 2025 down
Molm13-VR (Combo_DOWN)
CID131953885 EIF4A3-IN-2 HD-89-HC56 BAID12 10UM
eIF4A3 (RNA helicase) inhibitor
CID24748573 SILMITASERTIB IC-18-TY61 BAID24 10UM
CX-4945 (CK2 inhibitor)
CID126565 LESTAURTINIB RA-42-CM42 BAID47 1UM
Multi-targeted tyrosine kinase inhibitor
CID23582824 GSK-1059615 BF-22-EP86 BAID20 10UM
PI3K inhibitor
G
PDX 2016-7 (Combo_UP)
CID23582824 GSK-1059615 BF-22-EP86 BAID20 10UM
PI3K/mTOR dual inhibitor
CID49784945 IZORLISIB BF-26-MB27 BAID40 10UM
PIK3CA inhibitor
CID119182 CLOFARABINE CB-32-EI69 BAID20 10UM
purine nucleoside analog (chemotherapy)
CID5329102 SUNITINIB BB-09-GD09 BAID28 10UM
Multi-tyrosine kinase inhibitor
H
PDX 2016-7 (Combo_DOWN)
CID24748573 SILMITASERTIB IC-18-TY61 BAID24 10UM
CX-4945 (CK2 inhibitor)
CID23582824 GSK-1059615 BF-22-EP86 BAID20 10UM
PI3K/mTOR dual inhibitor

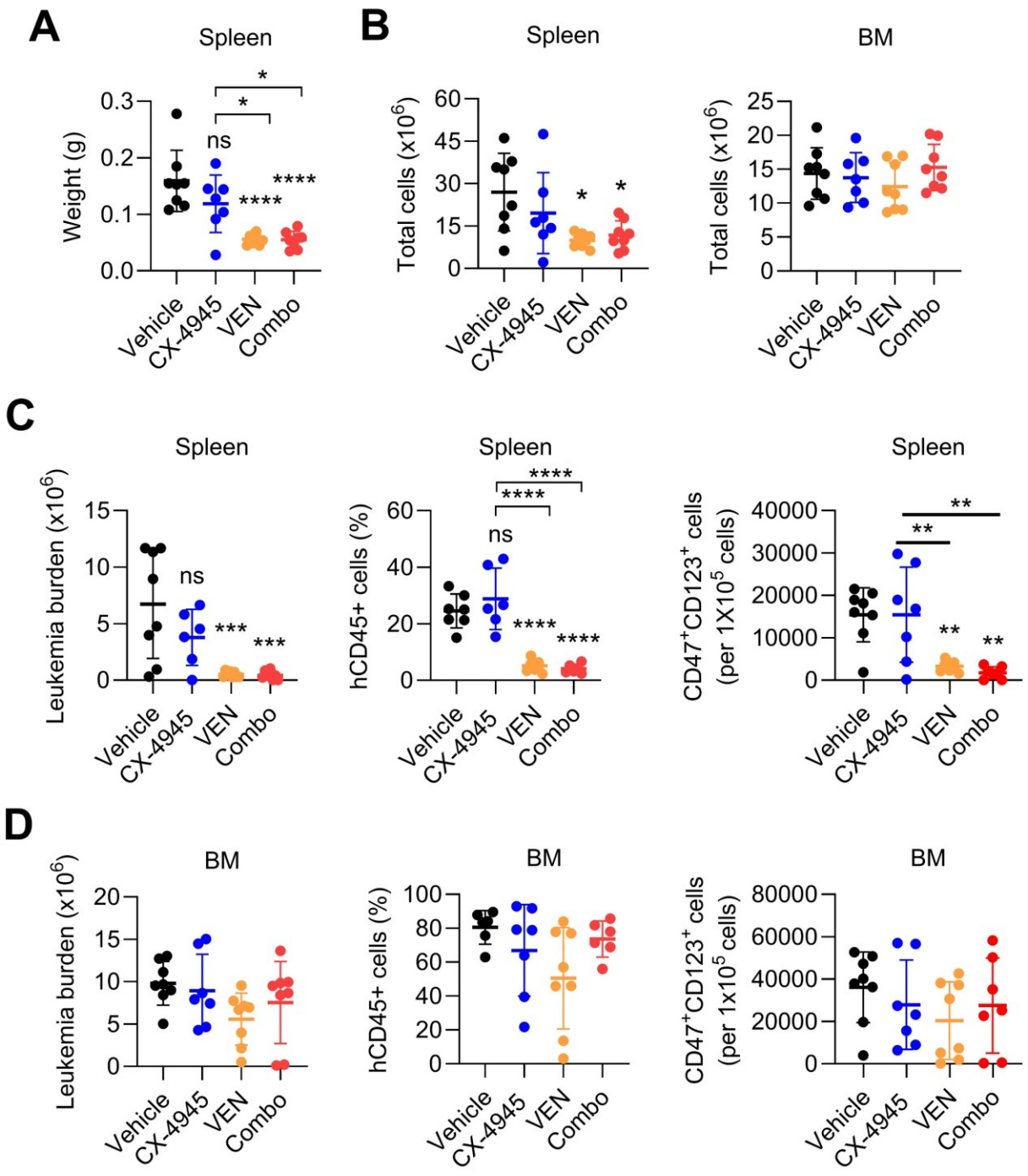
Supplementary Figure 7: Enrichment analyses of genes differentially regulated in Molm13-VR and PDX 2016-7 cells after treatment with CX-4945, VEN, and Combo. A-D) k-means clustering approach separated 623 MLL-r signature genes (adopted from references [8, 9]) based on their expression in Molm13 and Molm13-VR (**A**), and PDX 2016-7 cells (**C**). Subsequent enrichment analysis of different gene clusters obtained with k-means clustering of MLL-r genes showed top-ranked biological processes (gene ontology) in dot plot (**B, D**). **E-H)** DrugSeq (Drug perturbation signatures) enrichment analysis bar plot of DEGs obtained by Enrichr web tool. The genes upregulated (**E, G**) and downregulated (**F, H**) after treatment with CX+VEN combination in Molm13-VR (**E, F**) and 2016-7 PDX cells (**G, H**) were checked against most recent NIBR_DRUGseq_2025 gene-set libraries that significantly overlap with input genes. The length of the bar and intensity of the color represents the significance of that specific gene-set or term.


A
Flt3
MLL
IDH
Normal
PBMC
591
686
674
609
494
9190
9252
547
9194
9275
9215
AML ID#
kDa
p-CK2 sub
45
CK2α
26
BCL-XL
42
β-Actin
B
Basal level apoptosis in primary AML cells
Total Apoptosis (%)
AML patient cells
C
hCD38
hCD34
hTIM3
hCD34
hCD47
hCD123
674
494
609
686
9192
9215
D
FLT3-ITD
Normal Cyto
Apoptosis (relative to vehicle)
Veh
CX
VEN
CX+VEN
E
CD47+ (Chemoresistant)
F
hCD47 +ve population (relative to vehicle)

Supplementary Figure 8: The effect of CX-4945 in combination with VEN on primary AML cells. **A)** The basal level expression of CK2α, BCL-XL, and CK2 activity (p-CK2 substrate) was measured in primary AML cells by immunoblotting analysis. **B)** The basal level apoptosis and viability of primary AML patient cells was assessed after 12-24h of post-thaw using Annexin V & dead cell kit for Muse cell analyzer. The patient cells with high basal level apoptosis were omitted and the ones used for further testing were highlighted using red square box. **C)** AML cells from patients were surface stained with different fluorescent-labeled antibodies and analyzed for the expression of markers for LSCs (CD34, CD38, TIM3) and chemoresistance (CD47 and CD123) by flow cytometry. **D-F)** AML patient cells were treated with CX-4945 (2.5 μM) and VEN (0.5 μM) alone and in combination for 24 h and surface stained for different cell surface markers along with annexin V. The relative apoptosis in bulk cells (**D**) and chemoresistant (CD47+) subpopulations were calculated by normalizing the percent apoptosis in vehicle (Veh) treated cells (**E**). Also, the percentage of hCD47 positive AML cell population after drug treatment relative to vehicle (Veh) control was measured (**F**). The data are presented as mean ± SEM (n=6) and analyzed via one-way ANOVA (Tukey's multiple comparisons test) in '**E** & **F**'. *$p<0.05$ is considered as statistically significant.



Supplementary Figure 9: The effect of CX-4945 and VEN combination on complete blood count in mice xenografted with Molm13-VR, U937, and PDX 2016-7 cells. A-C) NRG-S mice transplanted with AML PDX 2016-7 cells ($0.5x10^6$ cells/mouse), Molm13-VR ($0.25x10^6$ cells/mouse), and U937 ($1x10^4$ cells/mouse) intravenously were treated with CX-4945, VEN, and Combo. After two-weeks of drug treatment, complete blood count (CBC) was analyzed from PDX 2016-7 (**A**), Molm13-VR (**B**) and U937 (**C**) CDX mice by Hemavet analyzer. Data are presented as mean ± SD (n=4-12). **p<0.01, ***p<0.001, and ****p<0.0001 by one-way ANOVA (Tukey's multiple comparisons test) denotes statistical significance.



Supplementary Figure 10: The effect of CX-4945 and VEN combination on leukemia burden in mice xenografted with PDX 2016-7 cells. A-D) NRG-S mice transplanted with AML PDX 2016-7 cells ($0.5x10^6$ cells/mouse) intravenously were treated with CX-4945, VEN, and Combo. After two weeks of drug treatment, xenograft mice were sacrificed and spleen weight was recorded (**A**). The cells collected from spleen and bone marrow were analyzed by flow cytometry for total cell number (**B**), leukemia burden, hCD45 positive cells, and chemoresistant cells (**C**, **D**). The data are presented as mean ± SD (n=7-8). *p<0.05, **p<0.01, ***p<0.001, and ****p<0.0001 by one-way ANOVA (Tukey's multiple comparisons test) denotes statistical significance.

Supplementary Tables

Table S1: Characteristics of AML cell lines.

Cell line	Source (Cat. No.)	Tissue	Disease	Age	Gender	Mutated genes	TP53 status
Molm13	DSMZ (ACC 554)	Peripheral blood	Acute myeloid leukemia	20 y	Male	FLT3-ITD, KMT2Ar	Wild-type
MV4-11	ATCC (CRL-9591)	Peripheral blood	Biphenotypic B Myelomonocytic Leukemia	10 y	Male	FLT3-ITD, KMT2Ar, MLL-AF4	Wild-type
OCI-AML3	DSMZ (ACC 582)	Peripheral blood	Acute myeloid leukemia	57 y	Male	DNMT3A, NPM1, NRAS	Wild-type
HL60	ATCC (CCL-240)	Peripheral blood	Acute promyelocytic leukemia	36 y	Female	CDKN2A, NRAS	deletion
K562	ATCC (CCL243)	Bone marrow	Chronic myelogenous leukemia	53 y	Female	BCR-ABL1	Mutated
THP-1	ATCC (TIB-202)	Peripheral blood	Acute monocytic leukemia	1 y	Male	NRAS, KMT2Ar	Mutated
U937	ATCC (CRL1593.2)	Pleural effusion, lymphocyte, myeloid	Histiocytic lymphoma	37 y	Male	PTEN, PTPN11, WT1	Mutated

Table S2: Characteristics of AML primary samples.

Sample ID	Diagnosis	Age (years)	Gender	Cytogenetics/Mutations
9252	AML	32	M	MLL-AF6
591	AML	62	F	FLT3-ITD, IDH1, KDM6A, NPM1, and DNMT3A
674	AML	58	M	FLT3-ITD, DNMT3A, and SMC3 mutated
609	AML	50	F	DNMT3A, TET2, NPM1, FLT3-ITD
686	AML	61	F	FLT3-ITD, DEK::NUP214
494	AML	60	M	FLT3-ITD, NPM1 mutations
9192	MDS/AML	64	F	no known high-risk alterations
9215	AML	62	M	no known high-risk alterations
547	MDS/AML	65	M	IDH2, NPM1, and SRSF2 mutations
590	AML	71	F	Complex karyotype, TP53
9190	AML	46	F	Complex karyotype; FLT3-ITD, DEK::NUP214
9194	AML	45	M	CBFB::MYH11
9275	AML	68	F	no known high-risk alterations
720	AML	52	F	Complex karyotype, DNMT3A, FLT3-TKD
9296	AML	30	M	no known high-risk alterations
9351	AML	32	M	no known high-risk alterations

Patient cells listed in shaded area (n=6) were used for the study. Other patient cells were omitted from study due to high basal level apoptosis and poor viability post-thaw.

Table S3: Characteristics of PDX AML cells.

Patient ID	PDX Model	Diagnosis	Age/Sex	MLL Status	Genetics	Reference
2017-38	AML-09	R/R AML	Unknown	MLL-r	MLL/AF9, NRAS	[9]
2016-1	AML-10	R/R AML	14y /F	Wildtype	CALM-AF10, TP53	[9]
2016-7	AML-18	R/R AML	16y /F	MLL-r	MLL/AF9	[9]
2017-14	AML-19	R/R tAML	6y /F	MLL-r	MLL/AF10	[9]

Table S4: Primers used for qPCR analysis.

Target	Forward primer (5' → 3')	Reverse primer (5' → 3')	Source
CK2α (*CSNK2A1*)	GGTGAGGATAGCCAAGGTTCTG	TCACTGTGGACAAAGCGTTCCC	IDT
CK2α' (*CSNK2A2*)	CGACCATCAACAGAGACTGACTG	GTGAGACCACTGGAAAGCACAG	IDT
BCL-XL (*BCL2L1*)	GCCACTTACCTGAATGACCACC	AACCAGCGGTTGAAGCGTTCCT	IDT
MCL1	CCAAGAAAGCTGCATCGAACCAT	CAGCACATTCCTGATGCCACCT	IDT
BAK	TTACCGCCATCAGCAGGAACAG	GGAACTCTGAGTCATAGCGTCG	IDT
BCL2A1	GGATAAGGCAAAACGGAGGCTG	CAGTATTGCTTCAGGAGAGATAGC	IDT
GAPDH	GTCTCCTCTGACTTCAACAGCG	ACCACCCTGTTGCTGTAGCCAA	IDT

Table S5: List of antibodies used for flow cytometry analysis of AML cells.

Target	Fluorochrome	Clone	Reference	Species	Provider
mCD45	BV711	30-F11	103147	Rat IgG2b, κ	BioLegend
hCD47	APC	B6H12	17-0479-42	Mouse IgG1, κ	eBioscience
hCD123	PE/Cy7	6H6	983702	Mouse IgG1, κ	BioLegend
hCD45	FITC	HI30	304006	Mouse IgG1, κ	BioLegend
hCD34	PE	581	343506	Mouse IgG1, κ	BioLegend
hCD38	APC/Cy7	HB-7	356616	Mouse IgG1, κ	BioLegend
hCD34	FITC	581	343504	Mouse IgG1, κ	BioLegend
hCD366 (Tim-3)	BV421	A18087E	364808	Mouse IgG1, κ	BioLegend

Table S6: List of antibodies used for immunoblotting analysis.

Target	Clone	Reference	Provider
CK2α	E-7	SC-373894	Santa Cruz Biotechnology
CK2α'	D-7	SC-514403	Santa Cruz Biotechnology
p-CK2 substrate		87385	Cell Signaling
p-AKT (S129)	D4P7F	13461s	Cell Signaling
pan-AKT	C67E7	4691s	Cell Signaling
BCL-XL	54H6	2764s	Cell Signaling
MCL-1 (detects L, S, ES isoforms)	D35A5	5453s	Cell Signaling
MCL-1 (detects only L isoform)	D5V5L	39224	Cell Signaling
BCL2A1 (A1/Bfl-1)	E3U2F	24951s	Cell Signaling
BAK	D2E11	5023s	Cell Signaling
BAX	D4E4	12105s	Cell Signaling
PARP		9542s	Cell Signaling
Cleaved Caspase-3 (Asp175)		9661s	Cell Signaling
β-actin	13ES	4970s	Cell Signaling
Gapdh	14C10	2118s	Cell Signaling

References:

1. Degnin, M., et al., *Novel Method Enabling the Use of Cryopreserved Primary Acute Myeloid Leukemia Cells in Functional Drug Screens.* J Pediatr Hematol Oncol, 2017. **39**(7): p. e359-e366.
2. Chou, T.C. and P. Talalay, *Quantitative analysis of dose-effect relationships: the combined effects of multiple drugs or enzyme inhibitors.* Adv Enzyme Regul, 1984. **22**: p. 27-55.
3. Rajaiah, R., et al., *CK2alpha Deletion in the Hematopoietic Compartment Shows a Mild Alteration in Terminally Differentiated Cells and the Expansion of Stem Cells.* Cells, 2025. **14**(13).
4. Tang, D., et al., *SRplot: A free online platform for data visualization and graphing.* PLoS One, 2023. **18**(11): p. e0294236.
5. Etoh, K. and M. Nakao, *A web-based integrative transcriptome analysis, RNAseqChef, uncovers the cell/tissue type-dependent action of sulforaphane.* J Biol Chem, 2023. **299**(6): p. 104810.
6. Kuleshov, M.V., et al., *Enrichr: a comprehensive gene set enrichment analysis web server 2016 update.* Nucleic Acids Res, 2016. **44**(W1): p. W90-7.
7. Olesinski, E.A. and S. Bhatt, *Dynamic BH3 profiling method for rapid identification of active therapy in BH3 mimetics resistant xenograft mouse models.* STAR Protoc, 2021. **2**(2): p. 100461.
8. Mullighan, C.G., et al., *Pediatric acute myeloid leukemia with NPM1 mutations is characterized by a gene expression profile with dysregulated HOX gene expression distinct from MLL-rearranged leukemias.* Leukemia, 2007. **21**(9): p. 2000-9.
9. Wunderlich, M., et al., *PDX models of relapsed pediatric AML preserve global gene expression patterns and reveal therapeutic targets.* bioRxiv, 2022: p. 2022.01.31.478534.